AD-A065 417 CERAMIC FINISHING CO STATE COLLEGE PA F/G 11/1
FRACTOGRAPHIC INVESTIGATION OF SUBCRITICAL CRACK GROWTH AT INHE--ETC(U)
NOV 78 H P KIRCHNER, R M GRUVER, D M RICHARD N00019-77-C-0328
UNCLASSIFIED NL

1 OF 2
AD
A065417

Ceramic Finishing Company
State College, Pennsylvania 16801

FRACTOGRAPHIC INVESTIGATION OF SUBCRITICAL CRACK GROWTH AT INHERENT FLAWS IN POLYCRYSTALLINE CERAMICS

November, 1978

Prepared by

Henry P. Kirchner
Robert M. Gruver
Dominique M. Richard

Prepared under Contract No. N00019-77-C-0328
for the Naval Air Systems Command, Department of the Navy

NOTE

This report contains several pairs of stereo scanning electron micrographs. Each left hand photograph is on the left and each right hand photograph is on the right. For viewing, the photographs should be cut out of the report and arranged with the correct spacing and orientation under a stereo viewer.

REPORT DOCUMENTATION PAGE

READ INSTRUCTIONS BEFORE COMPLETING FORM

1. REPORT NUMBER

2. GOVT ACCESSION NO

3. RECIPIENT'S CATALOG NUMBER

4. TITLE (and Subtitle)
Fractographic Investigation of Subcritical Crack Growth at Inherent Flaws in Polycrystalline Ceramics.

5. TYPE OF REPORT & PERIOD COVERED
Summary Report.
April 1977-November 1978

6. PERFORMING ORG. REPORT NUMBER

7. AUTHOR(s)
Henry P. Kirchner,
Robert M. Gruver
Dominique M. Richard

8. CONTRACT OR GRANT NUMBER(s)
N00019-77-C-0328

9. PERFORMING ORGANIZATION NAME AND ADDRESS
Ceramic Finishing Company
P.O. Box 498
State College, PA. 16801

10. PROGRAM ELEMENT, PROJECT, TASK AREA & WORK UNIT NUMBERS

11. CONTROLLING OFFICE NAME AND ADDRESS
Naval Air Systems Command
Code AIR 52032A
Washington, DC 20361

12. REPORT DATE
November, 1978

13. NUMBER OF PAGES
100

14. MONITORING AGENCY NAME & ADDRESS(if different from Controlling Office)
113p.

15. SECURITY CLASS. (of this report)

15a. DECLASSIFICATION/DOWNGRADING SCHEDULE

16. DISTRIBUTION STATEMENT (of this Report)

Distribution of this report is unlimited.

17. DISTRIBUTION STATEMENT (of the abstract entered in Block 20, if different from Report)

18. SUPPLEMENTARY NOTES

K SUB IC

K SUB I

19. KEY WORDS (Continue on reverse side if necessary and identify by block number)

ceramics, alumina, silicon nitride, fractography, fracture mechanics, subcritical crack growth, critical flaw boundaries, intergranular fracture, transgranular fracture, stress intensity factor, crack velocity, fracture mechanisms

20. ABSTRACT (Continue on reverse side if necessary and identify by block number)

Variations in intergranular and transgranular fracture along radii extending from fracture origins in hot pressed (H.P.) alumina, 96% alumina and H.P. silicon nitride were studied. The percent intergranular fracture (PIF) was plotted versus stress intensity factor (K_I) for various distances from the fracture origins assuming smooth crack fronts and the absence of localized stresses. The observed variations were analyzed in relation to single crystal and polycrystal K_{IC} values. The results were used to suggest fractographic criteria for subcritical crack growth boundaries in these materials.

DD FORM 1 JAN 73 1473 EDITION OF 1 NOV 65 IS OBSOLETE

79 03 05 024

404 419

SECURITY CLASSIFICATION OF THIS PAGE (When Data Entered)

LB

Ceramic Finishing Company
State College, Pennsylvania 16801

Fractographic Investigation of Subcritical Crack Growth at Inherent Flaws in Polycrystalline Ceramics

November, 1978

Prepared by:
Henry P. Kirchner
Robert M. Gruver
Dominique M. Richard

Prepared under Contract No. N00019-77-C-0328
for the Naval Air Systems Command, Department of the Navy

Table of Contents

Foreword

This summary report describes research performed on a program sponsored by the Naval Air Systems Command, Department of the Navy, under Contract N00019-77-C-0328. The research was performed under the general technical direction of Mr. Charles F. Bersch, Code AIR 52032A, of the Naval Air Systems Command.

The report covers work performed during the period 24 April 1977 to 23 October 1978. The authors are pleased to acknowledge the contributions of their associates at Ceramic Finishing Company.

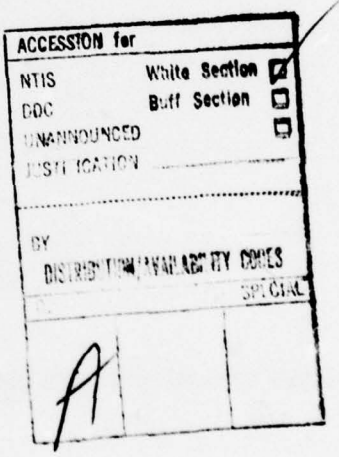

General Introduction

In polycrystalline ceramics the overall fracture process consists of a wide variety of elementary fracture processes including transgranular fracture of individual crystals on various crystal planes, intergranular fracture on various crystal surfaces, and fracture of intergranular phases. The polycrystalline fracture energy is the sum of the fracture energies (γ_F) of the elementary fracture processes.

The "mix" of the elementary fracture processes varies substantially along radii drawn from fracture origins in polycrystalline ceramics but the existence of these variations is not widely known and has been little studied. Presumably, in the early stages of slow crack growth, the first elementary fracture events to occur are those with the lowest γ_F such as fractures on $\bar{1}012$ planes in sapphire. As each such event occurs the stress intensity factor (K_I) at each intact grain at the crack front increases both as a result of the general increase in crack size and the tendency of the crack to advance around resistant grains. Because inherent flaws may not be large relative to the grain size, statistical factors governing the local distributions of grain sizes and orientations are likely to be important. Localized stresses arising from thermal expansion and elastic anisotropy are also important. One would expect the fracture to originate at the site that is most vulnerable in terms of the combination of flaw severity and reduced local critical stress intensity factor (K_{IC}).

The strength of ceramics is determined by the characteristics of preexisting flaws, subcritical crack growth, and the mechanism of transition

from subcritical to critical crack growth. Although, the mechanisms of fracture during critical crack propagation are interesting in their own right, these mechanisms are not relevant to the strength because at this stage the integrity of the ceramic article has been lost. Subcritical crack growth depends on the method of loading, the loading rate and the environment. At large cracks or flaws that experience average material properties, the crack velocity increases exponentially with increasing K_I. However, when the crack or flaw is so small that it does not experience such average properties, local conditions can be expected to have important influences on crack velocity. One would expect low loading rates and corrosive environments to favor more symmetrical advance of the crack front and more uniform increase in crack velocity. As K_I approaches K_{IC}, the crack accelerates to velocities in the range 10^{-4}-1 ms^{-1}. Fracture mechanics considerations alone do not lead us to expect any discontinuity in the fracture markings as the crack accelerates or at the critical crack growth boundary. The observed markings depend on the mechanisms of fracture of the particular material at each stage in the variation of K_I. Thus, resistance to fracture can result from the relative absence of flaws, resistance to subcritical crack growth which reduces the rate of increase of K_I or by the presence of obstacles that postpone the transition to critical crack propagation.

In this investigation, the variations in the elementary fracture processes along radii extending from fracture origins were studied in hot pressed (H.P.) alumina, 96% alumina, and H.P. silicon nitride by optical and scanning electron microscopy (SEM) including stereo SEM. The

variations in the relative frequencies of intergranular and transgranular fracture were determined. The percent intergranular fracture (PIF) was plotted versus K_I for various distances from the fracture origin assuming a smooth crack front and the absence of localized stresses. The observed variations were analyzed in relation to single crystal and polycrystal K_{IC} values.

The report has four main sections covering the following topics:

1. A fractographic criterion for subcritical crack growth boundaries in H.P. alumina.

2. Fracture mechanics of reflecting spots in H.P. alumina.

3. Fractographic criteria for subcritical crack growth boundaries in 96% alumina.

4. A Fractographic criterion for subcritical crack growth boundaries in H.P. silicon nitride.

The final section consists of general conclusions and recommendations.

A Fractographic Criterion for Subcritical Crack Growth Boundaries in Hot Pressed Alumina

by

H. P. Kirchner
R. M. Gruver

Ceramic Finishing Company
P.O. Box 498
State College, PA 16801

Acknowledgements

The authors are pleased to acknowledge the contributions of their associates at Ceramic Finishing Company. This research was sponsored by the Naval Air Systems Command under Contract N00019-77-C-0328.

Abstract

The percent intergranular fracture (PIF) was measured along radii extending from fracture origins in hot pressed alumina specimens, fractured at various loading rates and temperatures, and plotted versus estimates of stress intensity factors (K_I) at the various crack lengths. Minima in PIF occur at values of K_I that are close to the critical stress intensity factors (K_{IC}) for cleavage on various crystal lattice planes in sapphire. The subcritical crack growth boundary ($K_I = K_{IC}$ of the polycrystalline material) occurs near the primary minimum in PIF suggesting that this minimum can be used as a criterion for locating this boundary. In addition, it was noted that the polycrystalline K_{IC} (4.2 $MPam^{1/2}$) is very close to the K_{IC} for fracture on $\{\bar{1}\bar{1}26\}$ planes which is 4.3 $MPam^{1/2}$. These observations suggest that critical crack growth begins when increased fracture energy can no longer be absorbed by cleavage on these planes. There is a secondary minimum at $K_I > K_{IC}$ that appears to be associated with the K_{IC} necessary for fracture on combinations of planes selected by the fracture as alternatives to the high fracture toughness basal plane.

I. Introduction

Development of fracture theories and failure analysis has been handicapped by the lack of fractographic criteria for locating subcritical crack growth boundaries in fracture surfaces of ceramics. In this paper, such a criterion is described for hot pressed (H.P.) alumina.

It is well known that fracture origins in H.P. alumina, when observed in reflected light by optical microscopy, are surrounded by reflecting spots[1,2]. In fact, observation of these reflecting spots is the most reliable method of locating the fracture origins. The area of intense reflecting spots is related to the fracture stress and rate of loading[3]. In weak specimens or those fractured in delayed fracture, the areas are relatively large. In strong specimens or those fractured by impact, the areas are relatively small. Cleavage regions are observed surrounding flaws at fracture origins in H.P. alumina, 96% alumina and H.P. silicon nitride[3,4]. These cleavage regions are associated with subcritical crack growth[4,5]. These observations led to efforts to relate the reflecting spots in H.P. alumina to cleavage and a one to one correspondence was observed. Therefore, the reflecting spots and cleavage regions in H.P. alumina are associated with subcritical crack growth.

In an investigation of microplastic processes in a dense, coarse grained alumina, Lankford[6-8] was able to associate the acoustic emission recorded during subcritical crack growth with deformation twinning. The twinning process tends to propagate to adjacent grains and leads to microcrack formation. Therefore, twinning is one mechanism by which cleavage regions form in alumina.

The fracture energy of a crack traversing a polycrystalline ceramic is the sum of the fracture energies of the individual fracture events occurring near the crack front. These events include transgranular fracture on various crystal lattice planes in individual crystals having various orientations to the crack front, intergranular fracture on various crystal surfaces at various orientations to the crack front, and fracture of intergranular phases. It is well known that there can be substantial variations in the fracture energies for various crystal lattice planes of single crystals. Wiederhorn[9,10] measured the fracture energies (γ_F) for several crystal lattice planes in sapphire with the results given in Table I. Also included in the table are estimates of the critical stress intensity factors (K_{IC}) for the individual lattice planes calculated using $K_{IC} = (2E\ \gamma_F)^{1/2}$ in which E is Young's modulus which was assumed to be 407 GPa . These values of K_{IC} can be compared with K_{IC} for H.P. alumina which is about 4.2 $MPam^{1/2}$[11]. Becher[12] measured fracture energies in several additional planes showing that the fracture energies drop off rapidly for planes close to the basal (0001) plane.

The principal fracture events in H.P. alumina ceramics are cleavage on various crystal planes and intergranular fracture on various crystal surfaces. Because of the wide range of K_{IC} values of the individual cleavage events and knowing that cleavage and intergranular fracture are interpersed near the fracture origin, it is reasonable to expect that K_{IC} of the polycrystalline material will be characterized by a particular combination of cleavage and intergranular fracture events. Based on the above information, an attempt was made to relate the stress intensity factors (K_I) during subcritical crack growth to the critical stress intensity factors of the individual fracture events in the individual crystals and to develop a fractographic criterion for subcritical crack growth boundaries in H.P. alumina.

Table I. Fracture Energies[9,10] and Critical Stress Intensity Factors for Several Crystal Lattice Planes in Sapphire.

Fracture Plane	Fracture Energy Jm^{-2}	Critical Stress Intensity Factor $MPam^{1/2}$
$\bar{1}012$	6.0	2.15 (1.7)*
$10\bar{1}0$	7.3	2.4
$\bar{1}\bar{1}26$	24.4	4.3
0001	> 40	> 5.6

*See reference 10.

II. Procedures

The present research was done by fractographic analysis of H.P. alumina specimens fractured in earlier investigations. Preparation and testing of these specimens was described previously[4,5]. The specimens were cylindrical rods about 3.3 mm diameter, with densities ranging from 99.5 to 99.7% of theoretical and average grain size in the range 1-3 μm. The specimens were fractured in flexure.

The percentages of intergranular and transgranular fracture, along radii extending from the fracture origins, were determined using scanning electron micrographs (1000 or 2000 X) which were taken at intervals along the radii and assembled to form composite photographs of the fracture surfaces. A grid with spaces approximately equal to one grain size and ten spaces wide was prepared. The grid was placed on the composite photograph and the fracture surface at the center of each grid space was examined and classified as to whether it was intergranular or transgranular, characterizing a path about ten grains wide. This process was repeated for adjoining rows of the grid. The percentages of intergranular and transgranular fracture varied considerably from one row to the next so averages were calculated for each row which included the results of the preceding and following rows to form three row running averages.

The stress intensity factors were calculated for each row using the following equation for semi-circular surface cracks[13]

$$K_I = \frac{Y}{Z} \sigma_F (a)^{1/2} \qquad (1)$$

in which a is the crack depth, σ_F is the fracture stress, Y is a geometrical parameter (2 for surface flaws and 1.8 for internal flaws), and Z is a flaw shape parameter ($\frac{\pi}{2}$ = 1.57 for semicircular cracks). This equation assumes a planar crack. Furthermore, this equation is strictly correct only for delayed fracture specimens for which the applied stress is constant. For specimens fractured by a linearly increasing load, K_I is overestimated when $K_I < K_{IC}$ because the stress is overestimated. However, a computer simulation of crack growth in another alumina involving numerical integration of the crack velocities (V) using the empirical relation $V = AK_I^n$ revealed that 99% of the crack growth occurred in the last 6% of the time. Therefore, the error in the calculated K_I values is small for most of the crack growth.

Using the information from the procedures described above, curves of K_I vs. Percent Intergranular Fracture (PIF) were plotted.

In the initial attempts to determine the relationship between K_I and PIF, the results were scattered. There was no consistent relationship between K_{IC} for the individual fracture events and K_{IC} of the polycrystalline material. The problem seemed to arise because of uncertainties in the K_I values. A possible explanation was that in strong specimens in which there is a rapid variation in K_I with (a), small errors in locating the fracture origin were causing large errors in K_I. Therefore, weaker specimens were studied. More subcritical crack growth occurs in weak specimens and in delayed fracture specimens so that there is more gradual variation in fracture features. Also, more accurate K_I estimates could be made with specimens with well defined flaws at the fracture origins, symmetrical areas of reflecting spots and symmetrical fracture mirrors. Therefore, specimens with these characteristics were selected for investigation. The results are presented in the next section.

III. Results and Discussion

Fractures at room temperature, normal loading rate

Fracture surface of a specimen fractured in flexure by a linearly increasing load at a fracture stress of 436 MPa is shown in Figures 1 and 2. The fracture origin is a machining flaw about 15-20 μm deep. This flaw is bounded by a region of mainly transgranular fracture that appears as a dark spot at the top of the fracture surface in Figure 1. At higher magnification in Figure 2, the increase in transgranular fracture along the radius from the fracture origin, followed by a decrease in transgranular fracture, is evident. The K_I vs. PIF curve for this specimen is given in Figure 3. A horizontal dashed line indicates K_{IC} for the polycrystalline material. The minimum in PIF (maximum in percent transgranular fracture) almost coincides with K_{IC}.

Loading rate dependence

Specimens fractured by delayed fracture and by impact were measured. The loading rate variations were observed by comparing K_I vs. PIF curves for delayed fracture, normal loading rate and impact fractures.

The K_{IC} vs. PIF curve for a delayed fracture specimen fractured at 467 MPa in 362 seconds is given in Figure 4. This figure illustrates the increased detail observable in delayed fracture specimens. Again, there is a minimum in PIF near K_{IC}. Comparison of this curve with the previous one reveals another typical feature, a secondary minimum at about 5.6 $MPam^{1/2}$. Overall, the minima in PIF in Figure 4 occur at K_I

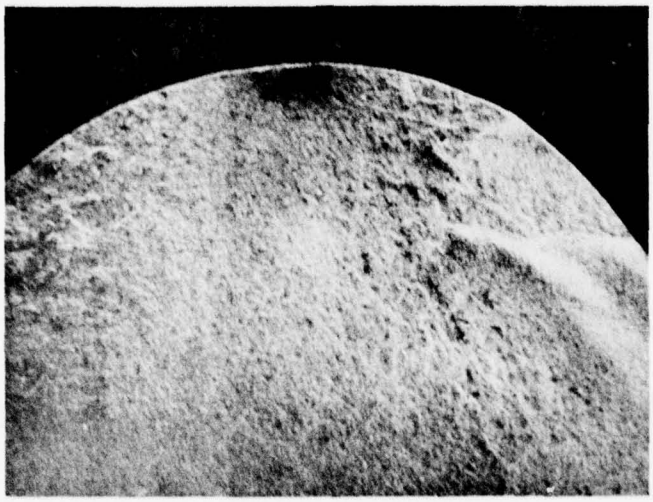

Figure 1 Hot Pressed Alumina (Specimen R-5) Fractured by a Linearly Increasing Load at 436 MPa (30 X).

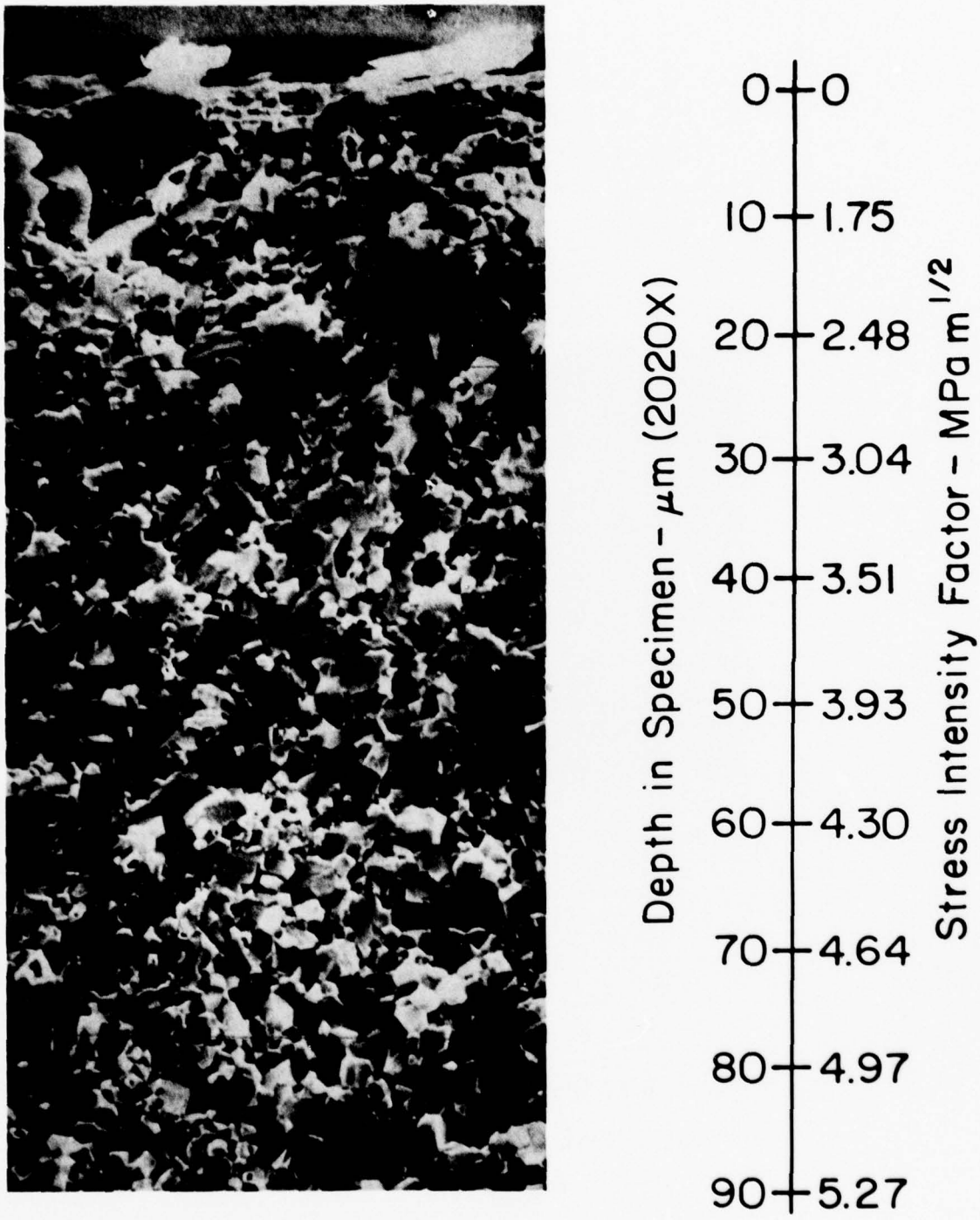

Figure 2 Hot Pressed Alumina (Specimen R-5) Fractured by a Linearly Increasing Load at 436 MPa (2020 X).

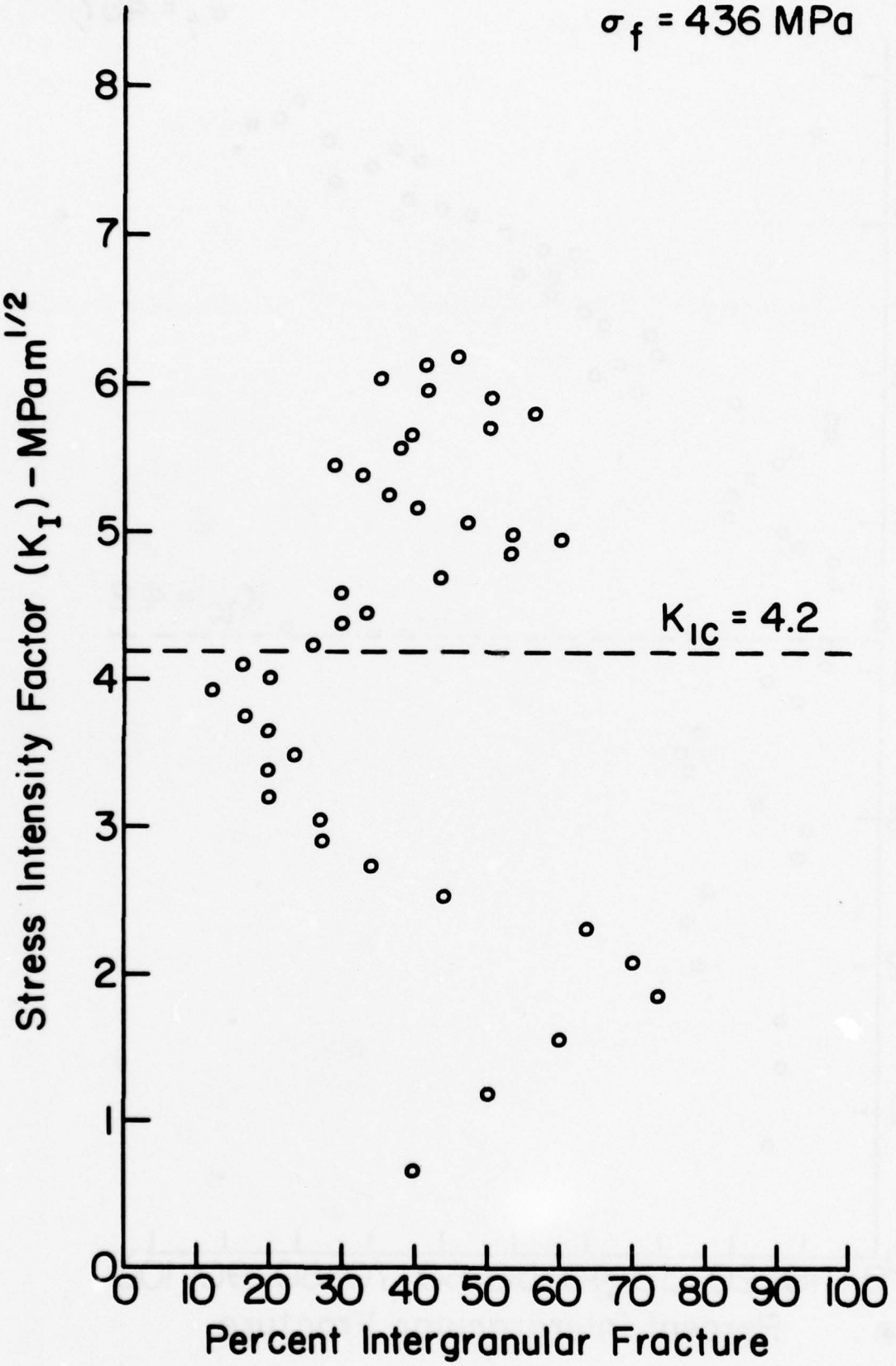

Figure 3 Stress Intensity Factor vs. Percent Intergranular Fracture, Linear Loading Rate (Hot pressed alumina, specimen R-5).

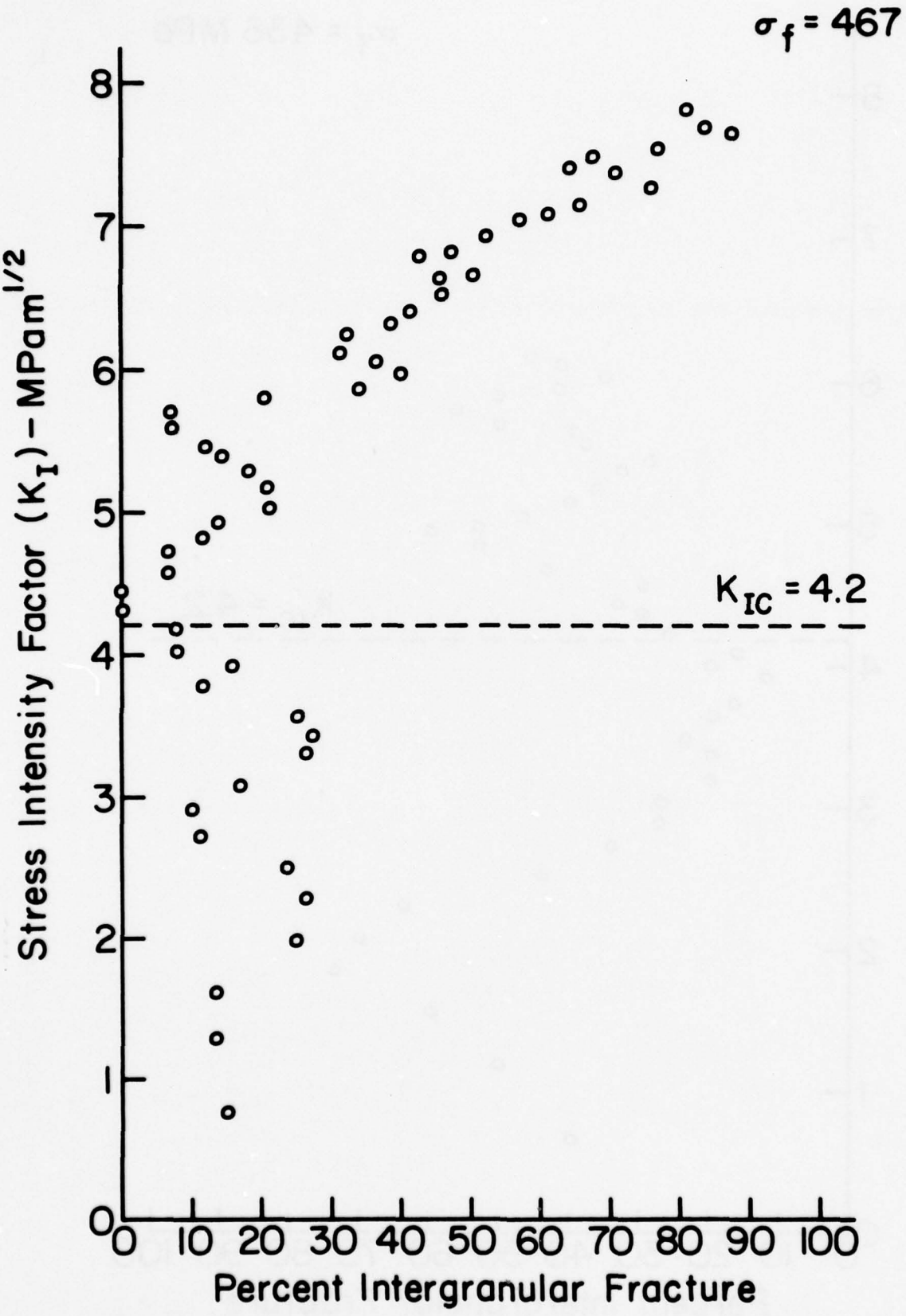

Figure 4 Stress Intensity Factor vs. Percent Intergranular Fracture, Delayed Fracture (Hot pressed alumina, specimen D-12).

values close to the K_{IC} values for various crystal lattice planes as listed in Table I.

There are definite differences between the curves in Figures 3 and 4 at low values of K_I. In this region ($K_I < 2$ MPam$^{1/2}$), the PIF depends on the type of flaw in each case. Machining flaws and surface pores have relatively high PIF. Large grains or groups of large grains acting as fracture origins tend to cleave, leading to relatively low values of PIF. When subsurface flaws are present, cleavage of the polycrystalline material between the flaw and the surface may indicate flaw linking[13] prior to fracture.

The K_I vs. PIF curve for specimen I-18 fractured by impact is given in Figure 5. The fracture stress is not measured directly during impact testing. Therefore, the fracture stress, necessary to compute K_I, was obtained from measurement of the fracture mirror radius using[14]

$$A = \sigma_F \, r_m^{1/2}$$

in which $A = 10.3$ MPam$^{1/2}$ [15] and r_m is the fracture mirror radius. The resulting fracture stress was 841 MPa. At the high loading rates characteristic of impact fractures there is much less subcritical crack growth than there is in the specimens fractured at lower loading rates. As a result, the fracture stresses are higher and variations in PIF occur close to the fracture origin and are obscured to some degree by the transition from the flaw to the subcritical crack growth region. These conditions result in a K_I vs. PIF curve in which the minor fluctuations are absent or poorly defined. Despite this fact, a definite minimum in PIF was observed at K_I close to K_{IC} of the polycrystalline material.

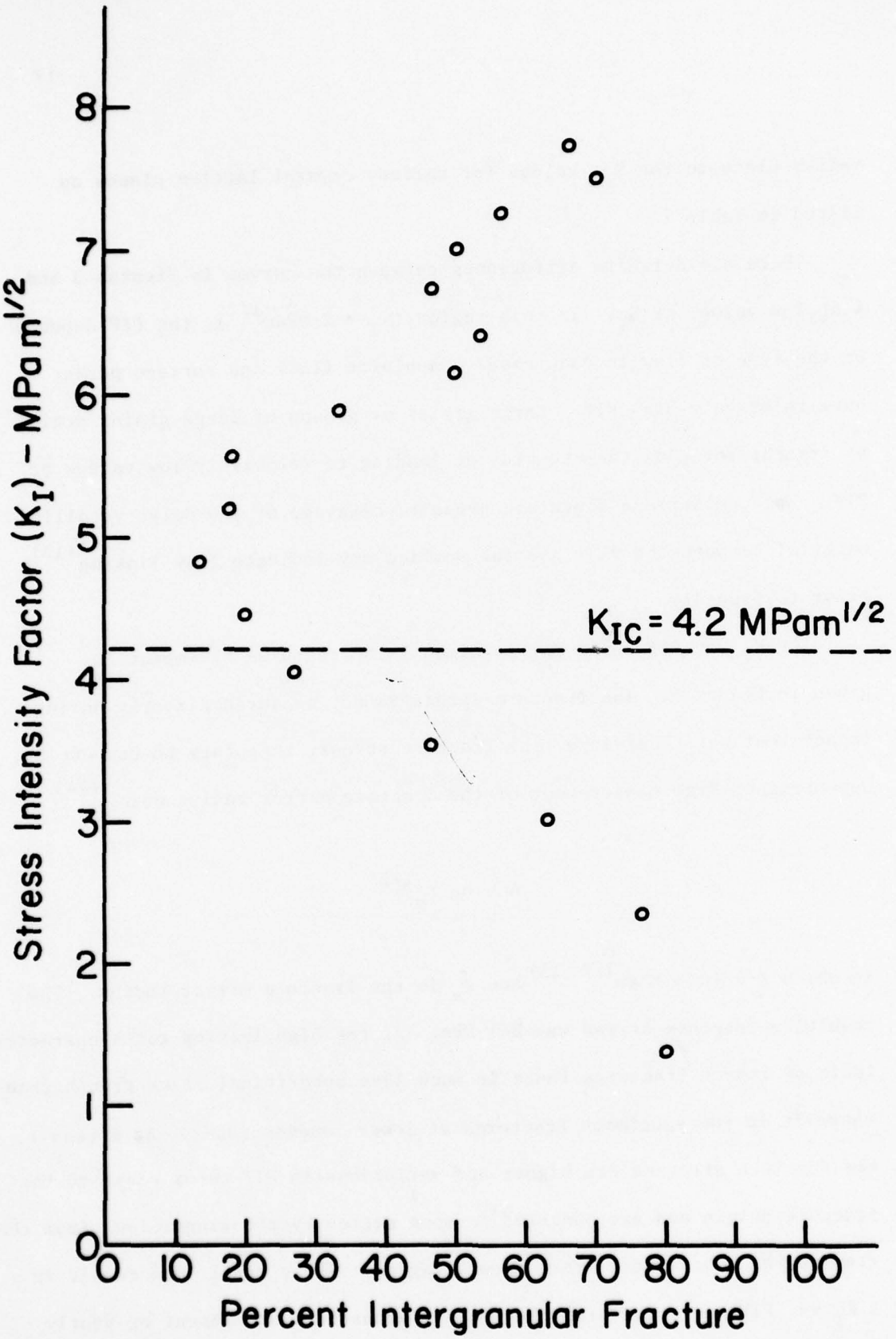

Figure 5 Stress Intensity Factor vs. Percent Intergranular Fracture, Impact Loading (Hot pressed alumina, specimen I-18).

Temperature dependence

Specimens fractured at elevated temperatures (800°C) were also measured. The results for a particular specimen (E-17), fractured at 528 MPa, are given in Figure 6. There is more intergranular fracture at 800°C than at room temperature but the shape of the curve remains roughly the same showing a primary minimum and secondary minima. Because K_{IC} values at elevated temperatures are not available it is not possible to compare K_I at minimum PIF with K_{IC}. However, if this K_I is taken as a criterion for the subcritical crack growth boundary, the fact that this K_I is still in the same range indicates that K_{IC} has not changed very much.

Lankford[7,8] indicates that twinning is more prevalent at elevated temperatures, that the twins are thicker, that there is multiple twin system activity, and that the onset of acoustic emission occurs at lower stresses. However, despite these facts, our observations indicate that there is less cleavage at high temperatures.

Perhaps the increased thickness of the twins and increased multiple twin system activity allow accommodation of more strain without cleavage thus leading to the higher fracture stresses observed in the temperature range 500-1000°C[16].

Discussion

The fact that the K_I at the lowest minimum in PIF coincides approximately with K_{IC} of the polycrystalline body suggests that the minimum in PIF (or the maximum in percent transgranular fracture) can be used as a

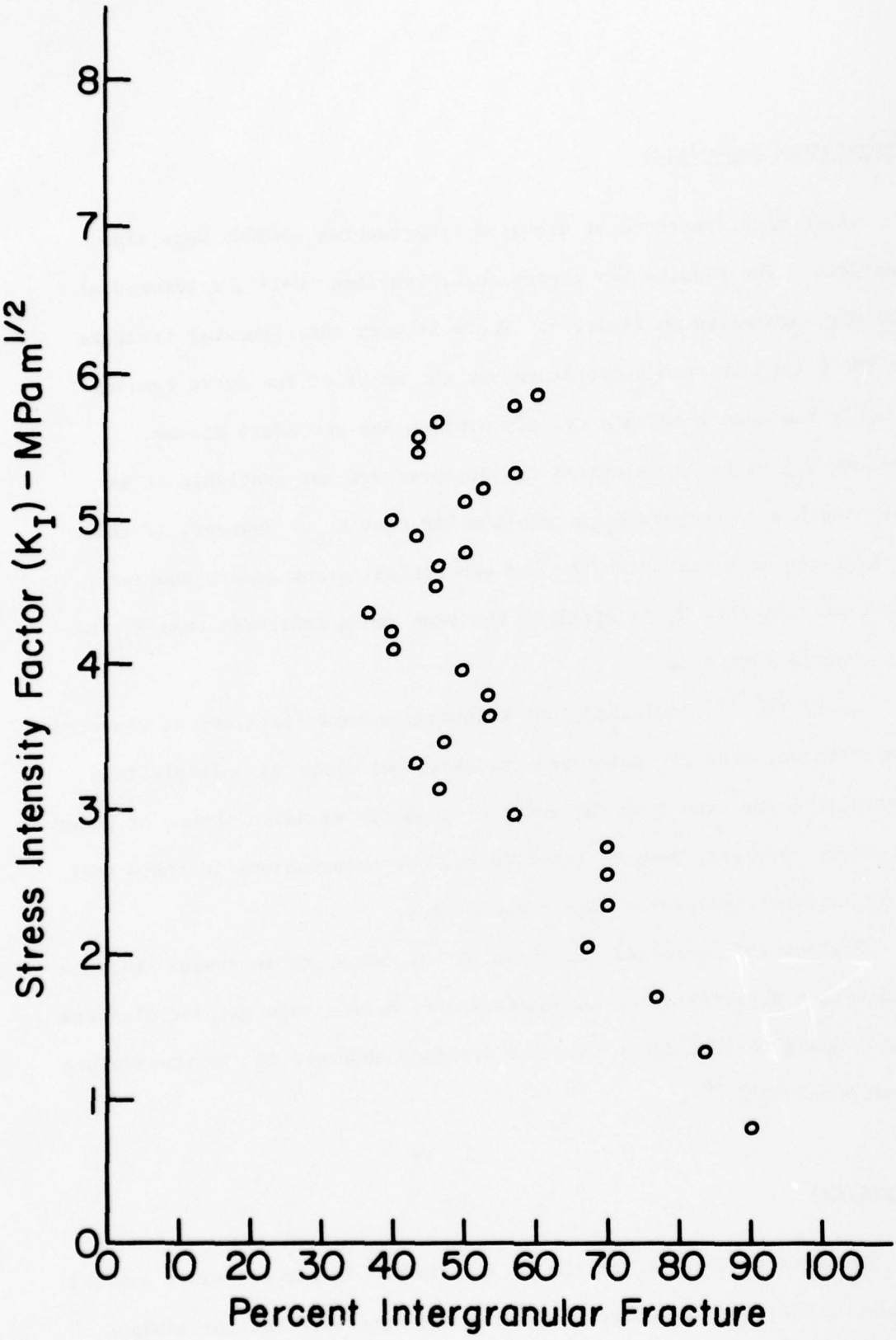

Figure 6 Stress Intensity Factor vs. Percent Intergranular Fracture, Linear Loading rate at 800°C (Hot pressed alumina, specimen E-17).

criterion to locate the subcritical crack growth boundary in fine grained H.P. alumina. Presumably, this criterion can be used to locate subcritical crack growth boundaries in fractures for which the fracture stress was not measured, making it possible estimate the fracture stress and stress distribution in such specimens. Also, the information should be helpful for calculating branching radius to critical flaw size ratios more precisely than has been done in the past. Determination of these ratios for various materials is important for the theory of crack propagation. The fact that K_{IC} almost coincides with K_I at the minimum in PIF, and considering that, at room temperature, almost all of the fracture at the subcritical crack growth boundary is transgranular suggests that critical crack growth begins when increased fracture energy can no longer be absorbed by cleavage on these lattice planes.

Comparison of the K_I vs. PIF curves with the K_{IC} values for the individual fracture events listed in Table I leads to interesting results. Based on the K_{IC} values for $\bar{1}012$ planes, one would expect crack growth to begin by cleavage on these planes of favorably oriented crystals at stresses of about 300-400 MPa (assuming a semicircular surface flaw with a radius of 20 μm). If the flaw is primarily intergranular, this will lead to decreasing PIF in the region surrounding the flaw (Figure 3). Apparently, intergranular fracture can also occur at these low stresses, perhaps aided by stress intensification at cleaved grains or by stress corrosion. As the crack depth and K_I increase, cleavage on other planes becomes possible. This

effect, plus the tendency for twinning to be propagated from one grain to the next, will cause further decrease in PIF. At K_I = 4.3 MPam$^{1/2}$ where all of the planes with measured values of K_{IC}, except (0001) can cleave the PIF is very low. Becher[12] has shown that basal twins induced by grinding cause small (0001) fracture surfaces in sapphire indicating that fracture on (0001) is possible even though it was not observed by Wiederhorn. However, twinning is a time consuming process[8]. A long extrapolation of Lankford's acoustic emission data indicates that strain rates of about 10^8 sec^{-1} would be required to suppress twinning (on all planes). Very high strain rates are present at the tips of running cracks. Therefore, it is not surprising that, as the crack accelerates near K_{IC}, the cleavage mechanisms gradually drop out and PIF increases.

One can speculate that the increase in PIF just above K_{IC} = 4.2 MPam$^{1/2}$ is limited by the increased availability of another cleavage mechanism as K_{IC} increases. This mechanism may be cleavage on $\{\bar{1}010\}$ combined with conchoidal fracture roughly parallel to $\{01\bar{1}4\}$ which occurs because of the difficulty of (0001) cleavage, as suggested by Wiederhorn[9]. In any case, the increase in PIF is reversed and with further increase in crack velocity and K_I, PIF passes through a secondary minimum at $K_I \cong$ 5.6 MPam$^{1/2}$. Above this value of K_I, PIF increases to high values (Figure 4).

The technique described in this paper requires very precise location of the fracture origin. For example, in the early stages of the investigation, specimen R-45 (σ_F = 660 MPa) was assumed to have a fracture origin at the surface. The K_I vs. PIF curve was determined and found to have a minimum in PIF at 6.6 MPam$^{1/2}$, by far the highest value observed thus far for H.P. alumina. On reexamination, the actual fracture origin was found

to be 19 μm below the surface. The K_I values were recalculated, assuming a subsurface penny-shaped flaw. The minimum in PIF is at about 4.8 $MPam^{1/2}$, a value that is now in the probable range of sample to sample variation of K_{IC}. Again, there is a secondary minimum at about 5.6 $MPam^{1/2}$.

The stress intensity factors at the minima in PIF for the H.P. alumina specimens investigated thus far are summarized in Table II. At room temperature the values of K_I at the lowest minimum in PIF near K_{IC} = 4.2 $MPam^{1/2}$ average 4.6 $MPam^{1/2}$ and occur at an average of 13% PIF. The values of K_I at the secondary minimum in PIF near K_I = 5.6 $MPam^{1/2}$ average 5.85 $MPam^{1/2}$ and occur at an average of 19% PIF.

In interpreting the above results it is important to realize that, first of all, the subcritical crack growth boundary and K_{IC} do not coincide with the boundary of the region of reflecting spots which consistently falls at higher values of K_I. Secondly, although the cleavage tends to form a reflecting region, it tends to terminate in a region of primarily intergranular fracture. There is no evidence of microbranching in this region of intergranular fracture. Therefore, the region of reflecting spots is not exactly analogous to the mirror region in glass because in that case the mirror region terminates in a region of microbranching usually called mist.

The fact that PIF varies with K_I leads one to consider whether or not PIF can be used to roughly estimate K_I at points on the fracture surface other than close to the fracture origin. Some steps were taken to evaluate this possibility. A substantial reduction in stress intensity factor is expected in the region of crack branching. A preliminary examination of fracture surfaces just before and just after crack branching

Table II. Stress Intensity Factors* at Minima in Percent Intergranular Fracture in Hot Pressed Alumina.

Specimen No.	Fracture Stress MPa	K_I and (PIF) at Minimum Near K_{IC} = 4.2 MPam$^{1/2}$	K_I and (PIF) at Minimum Near K_I = 5.6 MPam$^{1/2}$	Comments
Delayed Fracture Specimens				
D-13	458	4.6 (21%)	5.7 (24%)	
D-12	467	4.3 (0%)	5.7 (7%)	
Linear Loading Rate Specimens				
R-5	436	4.0 (13%)	5.6 (29%)	
R-13	477	4.9 (17%)	6.2 (30%)	
R-15	494	4.9 (20%)	6.0 (13%)	Primary and secondary minima are interchanged
R-21	See comments			Results rejected because of uncertainty in fracture stress
R-45	660	4.8 (8%)	5.9 (11%)	Subsurface fracture origin
	Average	4.6 (13%)	5.85 (19%)	
Impact Specimen				
I-18	841	4.8 (14%)	None	
Elevated Temperature Specimens				
		K_I at Minimum PIF		
E-17	528	4.3 (37%)	--	
E-11	461	3.9 (30%)	--	Subsurface fracture origin

*K_I calculated assuming a semi-circular flaw except for R-45 and E-11 for which an internal penny-shaped crack was assumed.

failed to reveal a substantial change in PIF. The fracture remained primarily intergranular. Therefore, one can conclude that K_I remains above K_{IC} during crack branching in H.P. alumina. This result is consistent with the observation of Döll[17] who found that the crack velocity decreases only slightly from the maximum crack velocity during branching in glass.

In flexural specimens K_I increases from the fracture origin to a maximum between 0.45 and 0.55 of the distance from the origin to the neutral axis[18,19] and then decreases. K_I vs. (a) curves extrapolate to $K_I = 0$ at about 1.4 to 1.6 of the distance from the origin to the neutral axis. Reflecting spots were observed at 1.2 of this distance. The area of reflecting spots was examined by SEM and was found to be caused by cleavage. Apparently, the stress intensity factor and crack velocity in this region were low enough so that the fracture was characterized by a distribution of types of individual fracture events like that occurring during subcritical crack growth near the fracture origin.

Preliminary evaluations of K_I vs. PIF curves for two other materials, 96% alumina and H.P. Si_3N_4, indicate that different fracture mechanisms occur at subcritical crack growth boundaries in these other materials. Therefore, one should expect different mechanisms and different criteria for the subcritical crack growth boundary in various ceramic materials.

The fact that the frequencies of various individual fracture events at K_{IC} are different from those at crack branching has implications for theories of crack propagation. Clearly, if there is a variation in the frequencies of individual fracture events with K_I, the fracture energy varies with crack velocity. In comparing the fracture energies at

criticality with those at crack branching, it is clear that, because there is no necessary relation between the distributions of the frequencies of the individual fracture events at criticality and at crack branching, there is no necessary relationship between fracture energies and thus no necessary relationship between K_{IC} and the stress intensity factor at crack branching (K_B). This result is important because it has been argued that there is a fixed ratio of crack branching radius to critical flaw size in various materials [20,21]. If this were correct it would imply that there is a direct proportionality between K_B and K_{IC} which would hold over a range of materials. However, it appears that this is not the case for the reasons given above.

The existence of correlations between K_{IC} and the types of individual fracture events occurring on the fracture surface, indicates some hope for development of improved methods of determination of K_{IC}. The best methods, currently in use, involve determination of the curve of crack velocity vs. K_I, selection of some arbitrary crack velocity usually in the range 10^{-4} - 1 ms^{-1}, and estimation of K_{IC} as the K_I value at this velocity. However, it is clear from the fractographic investigation described above that in H.P. alumina the crack grows subcritically until K_I becomes high enough for increased intergranular fracture to occur. Then, the structure "lets go" and failure occurs. In other materials the mechanisms may vary but they should be identifiable. Therefore, it may be desirable to define K_{IC} in terms of the change in the types of individual fracture events rather than in terms of an arbitrary crack velocity.

IV. Conclusions

1. The variations of PIF with K_I confirm that there is a relationship between the K_{IC} values of the individual fracture events and the types of fracture events occurring in H.P. alumina at particular values of K_I.

2. The subcritical crack growth boundary in H.P. alumina occurs near the lowest minimum in PIF (the maximum in transgranular fracture).

References

1. H. P. Kirchner, W. R. Buessem, R. M. Gruver, D. R. Platts, and R. E. Walker, "Chemical Strengthening of Ceramic Materials," Ceramic Finishing Company Summary Report, Contract N00019-70-C-0418, (December, 1970).

2. H. P. Kirchner, R. M. Gruver and R. E. Walker, "Strengthening of Hot-Pressed Al_2O_3 by Quenching," J. Amer. Ceram. Soc. 56 (1) 17-21 (1973).

3. H. P. Kirchner and R. M. Gruver, "Fracture Mirrors in Alumina Ceramics," Phil. Mag. 27 (6) 1433-1446 (1973).

4. R. M. Gruver, W. A. Sotter and H. P. Kirchner, "Fractography of Ceramics," Ceramic Finishing Company Summary Report, Contract N00019-73-C-0356 (November, 1974).

5. H. P. Kirchner, R. M. Gruver and W. A. Sotter, "Characteristics of Flaws at Fracture Origins and Fracture Stress-Flaw Size Relations in Various Ceramics," Mater. Sci. and Eng. 22, 147-156 (1976).

6. J. Lankford, "Compressive Strength and Microplasticity in Polycrystalline Alumina," J. Mater. Sci. 12, 791-796 (1977).

7. J. Lankford, Jr., "Microplasticity, Tensile Failure, and Indentation Damage in Unflawed Polycrystalline Alumina," Southwest Research Institute Technical Report, Contract N00014-75-C-0668 (April, 1977).

8. J. Lankford, Jr., "Compressive Microfracture and Indentation Damage in Alumina," from Fracture Mechanics of Ceramics, Vol. 3, Edited by R. C. Bradt, D. P. H. Hasselman, and F. F. Lange, Plenum, New York (1978).

9. S. M. Wiederhorn, "Fracture of Sapphire," J. Amer. Ceram. Soc. 52 (9) 485-491 (1969).

10. S. M. Wiederhorn, "Subcritical Crack Growth in Ceramics," from Fracture Mechanics of Ceramics, Vol. 2, Edited by R. C. Bradt, D. P. H. Hasselman, and F. F. Lange, Plenum, New York (1974) pages 613-646.

11. G. K. Bansal and W. H. Duckworth, "Effects of Specimen Size on Ceramic Strengths," from Fracture Mechanics of Ceramics, Vol. 3, Edited by R. C. Bradt, D. P. H. Hasselman and F. F. Lange, Plenum, New York (1978), page 190.

12. P. F. Becher, "Fracture-Strength Anisotropy of Sapphire," J. Amer. Ceram. Soc. 59 (1-2) 59-61 (1976).

13. A. G. Evans and G. Tappin, "Effects of Microstructure on the Stress to Propagate Inherent Flaws," Proc. Brit. Ceram. Soc. 20, 275-297 (June, 1972).

14. H. P. Kirchner, R. M. Gruver and W. A. Sotter, "Use of Fracture Mirrors to Interpret Impact Fractures in Brittle Materials," J. Amer. Ceram. Soc. 58 (5-6) 188-191 (1975).

15. H. P. Kirchner, "The Strain Intensity Criterion for Crack Branching in Ceramics," Eng. Fracture Mechanics 10, 283-288 (1978).

16. H. P. Kirchner and R. M. Gruver, "The Elevated Temperature Flexural Strength and Impact Resistance of Alumina Ceramics," Mater. Sci. and Eng. 13, 63-69 (1974).

17. W. Döll, "Investigations of Crack Branching Energy," Int. J. of Fracture 11, 184-186 (1975).

18. F. W. Smith, A. F. Emery and A. S. Kobayashi, "Stress Intensity Factors for Semicircular Cracks," Part 2 - Semi-Infinite Solid," J. Appl. Mech. 34, Series E, 953-959 (1967).

19. H. P. Kirchner and J. W. Kirchner, "Fracture Mechanics of Fracture Mirrors," To be published in J. Amer. Ceram. Soc.

20. J. J. Mecholsky, S. W. Freiman and R. W. Rice, "Fracture Surface Analysis of Ceramics," J. Mater. Sci. 11, 1310-1319 (1976).

21. G. K. Bansal and W. H. Duckworth, "Fracture Stress as Related to Flaw and Mirror Sizes," J. Amer. Ceram. Soc. 60 (7-8) 304-310 (1977).

Fracture Stress-Reflecting Spot Relations in Hot Pressed Alumina

by

H. P. Kirchner

D. M. Richard

Ceramic Finishing Company
P.O. Box 498
State College, PA 16801

Earlier observations have shown that the areas of the regions of intense reflecting spots, observed at fracture origins in alumina ceramics by optical microscopy, vary with fracture stress[1-5]. In weak specimens the areas are relatively large and in strong specimens they are relatively small.

The reflecting spots are caused by areas of transgranular fracture[2,6]. The fraction of transgranular fracture diminishes gradually with distance from the fracture origin[6,7] but the eye discerns a fairly definite boundary of reflecting spots. In members, uniformly stressed in tension, the stress intensity factor (K_I), at various points on the boundary of a semi-elliptical surface crack perpendicular to the stress (σ) is[8]

$$K_I = \frac{Y\,\sigma}{\Phi}\left(\frac{a}{c}\right)^{1/2}\left(a^2\cos^2\theta + c^2\sin^2\theta\right)^{1/4}$$

in which a and c are the semi-axes of the crack as indicated in Figures 1A and B, θ is the angle between the c-axis and a line joining the center of the ellipse with the point on the boundary for which K_I is calculated, Φ is the elliptic integral having the form

$$\Phi_1 = \int_0^{\pi/2}\left[1 - \left(1 - \frac{a^2}{c^2}\right)\sin^2\theta\right]^{1/2} d\theta,\quad a \leq c \qquad (2)$$

$$\Phi_2 = \frac{a}{c}\int_0^{\pi/2}\left[1 - \left(1 - \frac{c^2}{a^2}\right)\sin^2\theta\right]^{1/2} d\theta,\quad c \leq a \qquad (3)$$

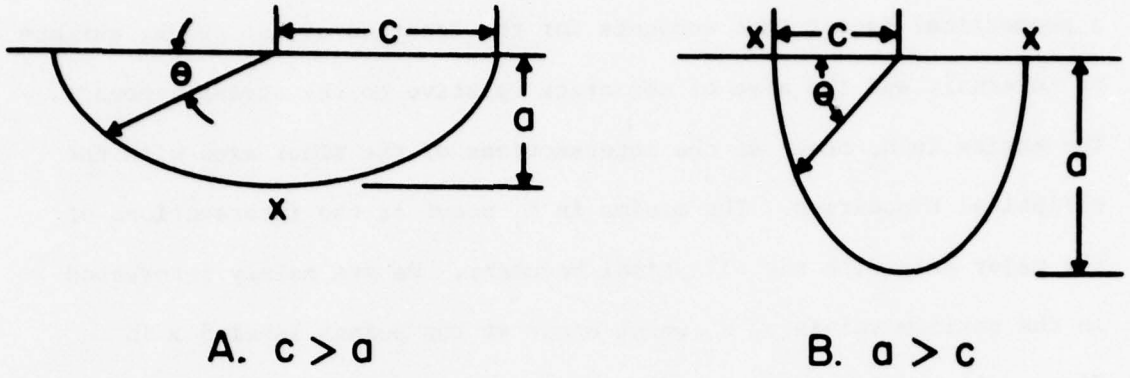

A. $c > a$ B. $a > c$

Figure 1 Semi-elliptical Surface Flaws

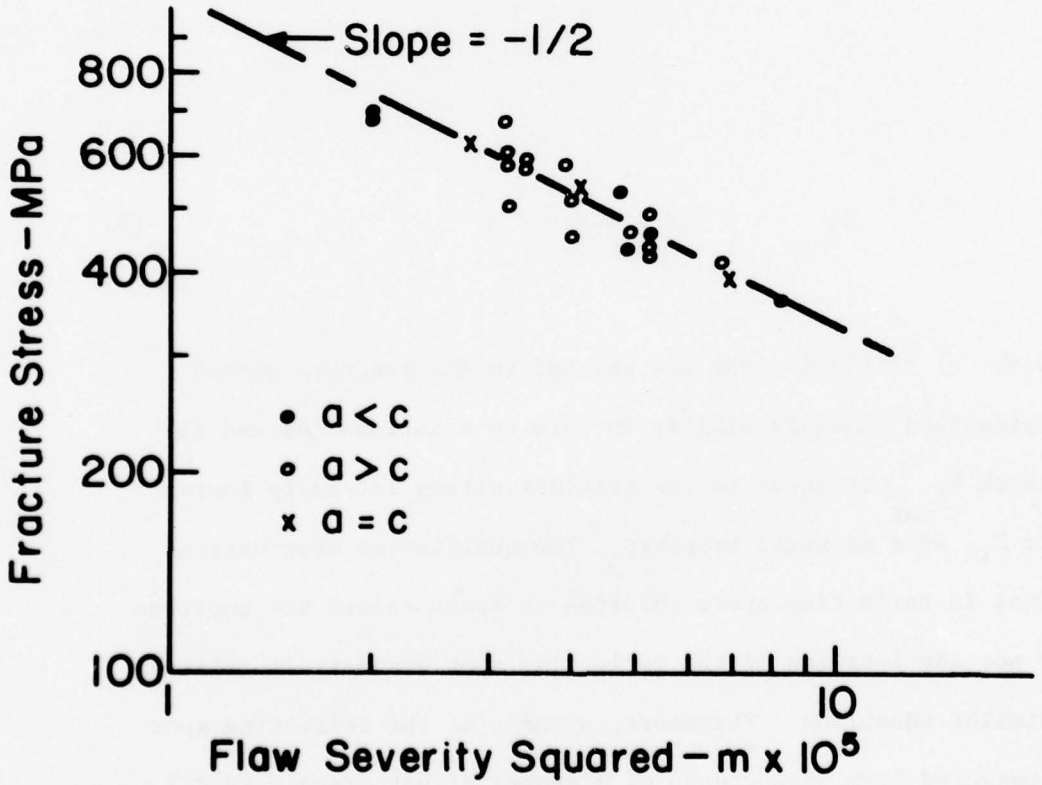

Figure 2 Fracture Stress vs. Flaw Severity Squared for Reflecting Spot Boundaries in H. P. Alumina Fracture in Flexure at Room Temperature.

so that $\Phi_2 = (\frac{a}{c})\ \Phi_1$, for a given eccentricity of the ellipse and Y is a geometrical factor that accounts for the location of the crack, surface or internal, and the size of the crack relative to the stressed member. The maxima in K_I occur at the intersections of the minor axes with the elliptical boundaries. The minima in K_I occur at the intersections of the major axis with the elliptical boundary. We are mainly interested in the maximum values of K_I which occur at the points labeled x in Figures 1A and B. Hence, we can compute these maximum values using

$$K_{I_{max}} = \frac{Y\ \sigma}{\Phi_1} \sqrt{a} \text{ for } c > a \tag{4}$$

and

$$K_{I_{max}} = \frac{Y\ \sigma}{\Phi_1} \sqrt{c} \text{ for } a > c \tag{5}$$

The sizes of critical flaws are related to the fracture stress (σ_f) by expressions that are similar in form to equations (4) and (5) above in which $K_{I_{max}}$ is equal to the critical stress intensity factor (K_{IC}) where K_{IC} is a material property. The qualitative observations of variations in reflecting spots referred to above raised the question whether or not the location of the reflecting spot boundary is related to σ_f by similar equations. Therefore, a and c of the reflecting spot area were measured from photographs of a number of hot pressed (H.P.) alumina specimens, 3.3 mm in diameter, fractured in flexure from surface

fracture origins in regular strength tests and by delayed fracture. The detailed procedures were described previously[3,4]. Although the applied stress field was non-uniform, the variation in stress across the reflecting spot region was negligible (less than about 10%).

If the flaw severity is defined as the square root of the length of the minor semi-axis divided by Φ_1, it is a measure of the greatest stress intensification at a crack. Rearranging (5) and taking the logarithm of the terms yields

$$\log \frac{K_I}{Y} = \log \sigma + \frac{1}{2} \log \frac{C}{\Phi_1^2} \tag{6}$$

Therefore, if we assume that there is a particular maximum value of the stress intensity factor, say K_R, at which the reflecting spot boundary forms along the minor axis, a plot of the fracture stress (σ_f) vs. the flaw severity squared should have a slope of -1/2. Such a plot for H.P. alumina specimens fractured in flexure is given in Figure 2. Values of Φ_1 were taken from mathematical tables. A dashed line with a slope of -1/2 has been drawn through the data. Clearly, the slope indicated by the data is close to -1/2. K_R was estimated at a value of C/Φ_1^2 of $4.5 \cdot 10^{-5}$ m, using Y = 2.0 for surface cracks yielding K_R = 6.6 MPam$^{1/2}$. The critical stress intensity factor (K_{IC}) of a similar alumina body was measured by Bansal and Duckworth[9] and found to be 4.2 MPam$^{1/2}$. Therefore, K_R is substantially greater than K_{IC} showing that the reflecting spot boundary is not the subcritical crack growth boundary.

The average value of the stress intensity factor at the intersection of the major axis with the boundary of the reflecting spots ($K_{I_{min}}$) was calculated yielding 5.5 $MPam^{1/2}$. This value is also greater than K_{IC}. The variation in K_I along the reflecting spot boundary is substantial and is clearly different from the constant values of K_I observed along crack branching boundaries [10,11]. This observation points out a contradiction involved in characterizing the area of reflecting spots as the "inner mirror"[5]. If the area of reflecting spots were associated with crack branching as implied by this characterization, K_I should be constant around the boundary.

Bansal[8] has shown that the areas of critical flaws (A) are related to the fracture stress by

$$\sigma_f \cong \frac{1.68}{Y} \frac{K_{IC}}{A^{1/4}} \qquad (6)$$

By analogy, one might expect a similar relation to hold for the areas of ellipses formed by reflecting spot boundaries. The area of an ellipse is πac so that for a semi-ellipse $\frac{2}{\pi} A = ac$. The log of σ_f is plotted vs. $\log \frac{2}{\pi} A$ in Figure 3. The slope is -1/4, as expected.

The results for delayed fracture specimens were analyzed similarly. The average K_R calculated at the minor axis intersections was 6.6 $MPam^{1/2}$, confirming the above result and showing that the observed increase in the area of the reflecting spots in delayed fracture specimens is a result of the lower fracture stresses caused by subcritical crack growth rather than being a direct result of loading rate. The

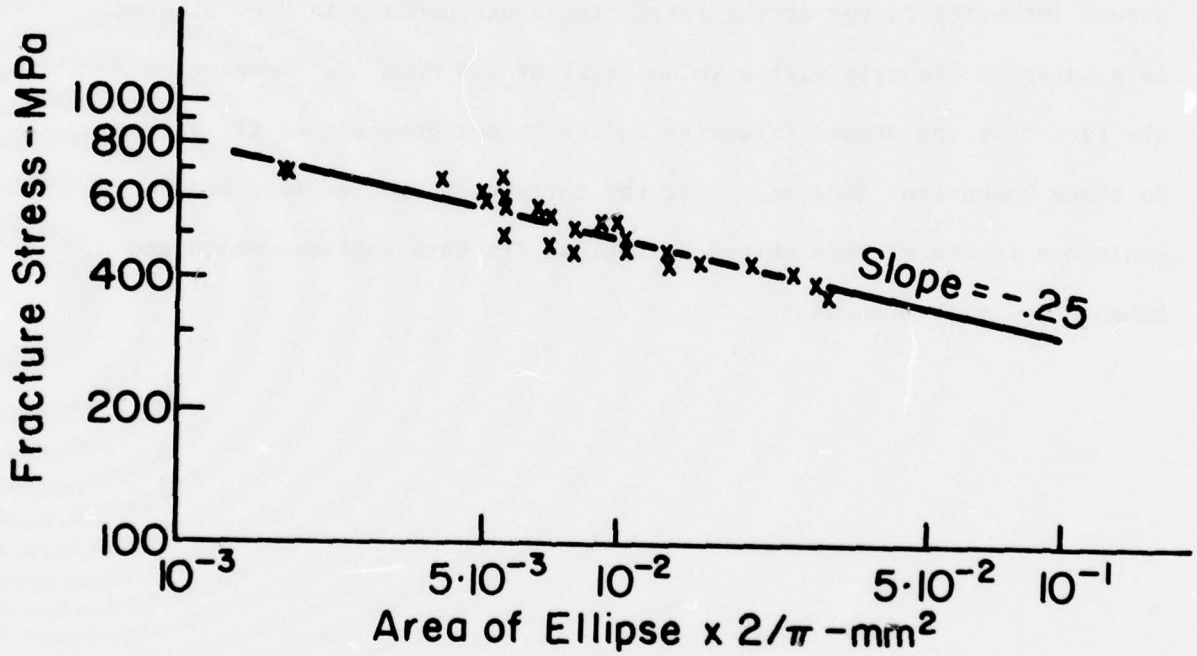

Figure 3 Fracture Stress vs. Area of Ellipse x $2/\pi$ Formed by Reflecting Spot Boundaries in H.P. Alumina Fractured in Flexure at Room Temperature.

c-axes of the ellipses formed in delayed fracture specimens appear to be greater on the average relative to the a-axes, compared with the specimens fractured in regular strength tests. This difference may have occurred as a result of stress corrosion enhanced crack growth along the surface.

In conclusion, it has been shown quantitatively that the maximum stress intensity factor at the reflecting spot boundary in H.P. alumina is a material property with a value of about 6.6 $MPam^{1/2}$. However, the fact that the stress intensity factor is not constant at all points on these boundaries indicates that the reflecting spot regions are not analogous to the mirrors observed in glass fracture surfaces which are bounded by crack branching.

References

1. H. P. Kirchner, W. R. Buessem, R. M. Gruver, D. R. Platts and R. E. Walker, "Chemical Strengthening of Ceramic Materials," Ceramic Finishing Company Summary Report, Contract N00019-70-C-0418, (December, 1970).

2. H. P. Kirchner and R. M. Gruver, "Fracture Mirrors in Alumina Ceramics," Phil. Mag. 27 (6), 1433-1446 (1973).

3. R. M. Gruver, W. A. Sotter and H. P. Kirchner, "Fractography of Ceramics," Ceramic Finishing Company Summary Report, Contract N00019-73-C-0356 (November, 1974).

4. H. P. Kirchner, R. M. Gruver and W. A. Sotter, "Characteristics of Flaws at Fracture Origins and Fracture Stress-Flaw Size Relations in Various Ceramics," Mater. Sci. and Eng. 22, 147-156 (1976).

5. R. W. Rice, "Fractographic Identification of Strength Controlling Flaws and Microstructure," from Fracture Mechanics of Ceramics, Vol. 1, Edited by R. C. Bradt, D. P. H. Hasselman and F. F. Lange, Plenum, New York (1974), pages 323-345.

6. H. P. Kirchner and R. M. Gruver, "Fractographic Criteria for Subcritical Crack Growth Boundaries in 96% Alumina," To be submitted for publication.

7. H. P. Kirchner and R. M. Gruver, "A Fractographic Criterion for Subcritical Crack Growth Boundaries in Hot Pressed Alumina," Submitted for publication.

8. G. K. Bansal, "Effect of Flaw Shape on the Strength of Ceramics," J. Amer. Ceram. Soc. 59 (1-2), 87-88 (1976).

9. G. K. Bansal and W. H. Duckworth, "Effects of Specimen Size on Ceramic Strengths," from Fracture Mechanics of Ceramics, Vol. 3, Edited by R. C. Bradt, D. P. H. Hasselman and F. F. Lange, Plenum, New York (1978), pages 189-204.

10. H. P. Kirchner, "The Strain Intensity Criterion for Crack Branching in Ceramics," Eng. Fracture Mechanics 10, 283-288 (1978).

11. H. P. Kirchner and J. W. Kirchner, "Fracture Mechanics of Fracture Mirrors," To be published in J. Amer. Ceram. Soc.

Fractographic Criteria for Subcritical Crack Growth Boundaries in 96% Alumina

by

H. P. Kirchner

R. M. Gruver

Ceramic Finishing Company
P.O. Box 498
State College, PA 16801

Abstract

The percent intergranular fracture (PIF) was measured along radii extending from fracture origins in 96% alumina specimens, fractured at various loading rates and temperatures, and plotted versus estimates of stress intensity factors (K_I) at the corresponding crack lengths. Two types of curves were observed. The first type was similar to curves previously observed for hot pressed alumina. In this case the subcritical crack growth boundary was located approximately where the minimum in the PIF occurred near $K_I = 4\ MPam^{1/2}$ as was also the case for hot pressed alumina. Therefore, the location of this minimum or the projecting grains formed by intergranular fracture as the crack velocity increased can be used as criteria for locating the subcritical crack growth boundary. The second type of curve lacks the minima in PIF characteristic of the first type and is characterized by a gradual trend toward higher PIF beginning at $K_I \gtrsim 3MPam^{1/2}$. This type of curve may be caused by acceleration of the crack to high crack velocities at values of K_I approximately equal to or slightly greater than those necessary to cause critical crack growth on the lower fracture energy planes in sapphire. Assuming that this is the case, one can use the K_I at which the trend toward higher PIF begins to calculate the radius to the critical flaw boundary for this type of fracture.

I. Introduction

Previous research has shown that, in polycrystalline alumina ceramics, fractures originate at several types of preexisting flaws[1-7]. Attempts to correlate the flaw sizes and the fracture stresses of individual specimens have achieved only partial success. The principal reason for the difficulties is that subcritical flaw growth increases the size of the preexisting flaws. When fracture stress (σ_f) is estimated using[2]

$$\sigma_f = \frac{Z}{Y} \frac{K_{IC}}{a^{1/2}} \tag{1}$$

in which K_{IC} is the critical stress intensity factor, a is the flaw size, Z is the flaw shape parameter and Y is a geometrical factor accounting for the flaw location and the relative sizes of the flaw and specimen, substitution of the sizes of pores, large crystals or other flaws at the fracture origins yields overestimates of the fracture stress because of failure to account for subcritical crack growth. One cannot accurately calculate these fracture stresses without reliable evidence of the flaw size and shape when the stress intensity factor (K_I) equals K_{IC}.

One way to determine the critical flaw size and shape is to determine a fractographic criterion for the critical flaw boundary so that, by applying such a criterion, the critical flaw can be outlined by post mortem fractographic examination. Bansal, Duckworth and Niesz[7] used calculations based on measured fracture stresses and assumed flaw shapes to draw critical flaw boundaries on a small number of fracture surfaces in

96% alumina. These boundaries appeared to coincide with fracture features. Kirchner and Gruver[8] developed a fractographic criterion for subcritical crack growth boundaries in hot pressed (H.P.) alumina based on the variation of the ratio of intergranular to transgranular fracture with K_I.

In this investigation, fracture surfaces of 96% alumina specimens were characterized by optical and scanning electron microscopy (SEM), including stereo SEM. The results were used to suggest fractographic criteria for subcritical crack growth boundaries in this material.

II. Procedures

96% alumina specimens*, fractured in earlier investigations, were analyzed by fractography. Preparation and testing of these specimens was described previously[1,5]. The specimens were cylindrical rods, 3.2 mm diameter, with a specific gravity of 3.71 and average grain size in the range 5-7 μm.

The percentages of intergranular and transgranular fracture, along radii extending from the fracture origins, were determined using scanning electron micrographs (1000 or 2000 X) which were taken at intervals along the radii and assembled to form composite photographs of the fracture surfaces. A grid with spaces approximately equal to one grain size at 2000 X and ten spaces wide was prepared. The grid was placed on the composite photograph and the fracture surface at the center of each grid space was examined and classified as to whether it was intergranular or transgranular, characterizing a path about ten grains wide. This process was repeated for adjoining rows of the grid. The percentages of intergranular and transgranular fracture varied considerably from one row to the next so averages were calculated for each row which included the results of the preceding and following rows to form three row running averages.

The stress intensity factors were calculated for each row using the following equation for semi-circular surface cracks[2]

$$K_I = \frac{Y}{Z} \sigma_f \, (a)^{1/2} \qquad (2)$$

---

*ALSIMAG 614, 3M Company, Chattanooga, Tenn.

in which a is the crack depth, σ_F is the fracture stress, Y is a geometrical parameter (2 for surface flaws and 1.8 for internal flaws), and Z is a flaw shape parameter ($\frac{\pi}{2}$ = 1.57 for semicircular cracks). This equation assumes a planar crack. Furthermore, this equation is strictly correct only for delayed fracture specimens for which the applied stress is constant. For specimens fractured by a linearly increasing load, K_I is overestimated when $K_I < K_{IC}$ because the stress is overestimated. However, a computer simulation of crack growth in this alumina involving numerical integration of the crack velocities (V) using the empirical relation $V = AK_I^n$ revealed that 99% of the crack growth occurred in the last 6% of the time. Therefore, the error in the calculated K_I values is small for most of the crack growth. The equation was suitably modified when it was applied to internal penny-shaped cracks. Using the information from the procedures described above, curves of K_I vs. Percent Intergranular Fracture (PIF) were plotted and analyzed.

III. Results and Discussion

A. Fractography of 96% alumina

Fractographic examinations can be used to locate and characterize flaws at fracture origins and to establish relationships between fracture features and the stress intensity factor acting at the crack tip at each point during crack propagation, for various loading conditions (loading rate, temperature and environment). In the following paragraphs these relationships will be discussed for reflecting spots, transgranular fracture at adjacent grains, and subcritical crack growth at pores.

Reflecting spots

It is well known that fracture origins in alumina ceramics are surrounded by fracture features that reflect incident light called reflecting spots[1,3,4,9]. Reflecting spots in one half of a specimen correspond in detail to reflecting spots in the other half as shown in Figure 1. Therefore, one might anticipate that the reflecting spots are caused by reflections from regions of transgranular fracture because these features are normally the only features with the same appearance in both halves of the specimen. That this is the case is illustrated in Figure 2 where the regions of transgranular fracture surrounding the pore are, after allowing for the small difference in magnification, identical in size and shape to the reflecting spots. It should be noted that not all of the regions of transgranular fracture can be in the reflecting position at one orientation but that small changes in orientation would cause the other regions of transgranular fracture to reflect.

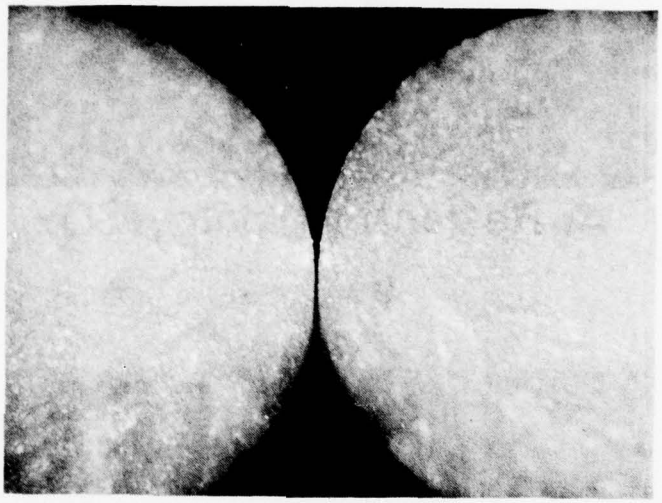

Figure 1 Comparison of reflecting spots in both halves of a 96% alumina specimen (Specimen AR-2, fractured in flexure at room temperature at 434 MPa).

A. Reflecting spots, 160x

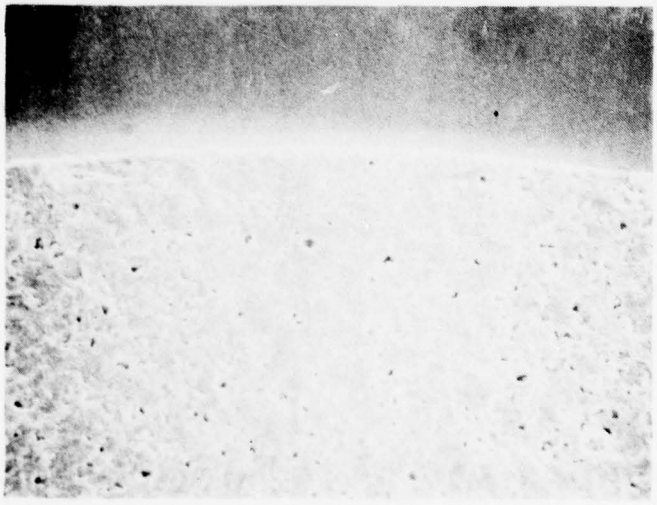

B. Areas of transgranular fracture, 200x

Figure 2 Comparison of reflecting spots and areas of transgranular fracture in 96% alumina (Specimen N-37 fractured at -196 °C)

The area of reflecting spots varies with fracture stress and loading rate. The areas are relatively large for weak specimens or those loaded at low loading rates and relatively small for those that are strong or loaded at high loading rates[9]. These observations lead one to associate reflecting spots and transgranular fracture with subcritical crack growth. However, the area of reflecting spots is not the region of subcritical crack growth because calculations of the stress intensity factors at the reflecting spot area boundaries yield values of K_I that are greater than K_{IC}.

At a given fracture stress there is a greater area of reflecting spots when fracture originates at a pore than there is when fracture originates at other types of flaws. This difference is particularly great in the case of fractures at -196°C or under impact loading. It may be caused by the fact that pores are less effective stress concentrators than other types of flaws so that substantial subcritical crack growth must occur before the combined pore and crack act as a sharp crack. Evans and Tappin[2] have shown that this does not happen until the crack grows to a length equal to 0.3 of the pore radius. Pores as large as 75 μm in radius have been observed at fracture origins in 96% alumina so that 25 μm of additional subcritical crack growth is required in this case.

The above observations of reflecting spots and their association with transgranular fracture suggest that significant observations should result from investigation of the variations of transgranular and intergranular fracture in 96% alumina.

Transgranular fracture of adjacent grains

It is clear from examination of the fracture surfaces that many of the areas of transgranular fracture are much larger than the average grain size. This observation raises the question whether these areas traverse only a single large grain or, instead, several grains fracture on a single plane. One way to obtain evidence relevant to this question is to examine the intersections of these areas of transgranular fracture with thermally etched surfaces as shown in Figure 3. In this case the fracture originated at a pore and a large grain slightly below the surface. The thermally etched surface indicates the grain size of the body and it is evident that the specimen surface near the large grain contains many grains having a normal range of sizes. However, the region of transgranular fracture extends to the surface with little deviation from the plane of fracture of the large crystal. Similar observations have been made at the edges of pores. Therefore, it is clear that regions of transgranular fracture can spread from grain to grain with little change in direction. As shown by Becher[10], the fracture energies vary only slightly over a wide range of crystallographic directions in sapphire. It is only when the crack is attempting to propagate in directions near the basal plane that there is substantial increase in fracture energy. Therefore, it is not surprising that cracks can propagate transgranularly over large distances in polycrystalline alumina ceramics with little change in direction.

The mechanism by which the transgranular fracture spreads from one grain to another has not yet been established. However, Lankford[11-13]

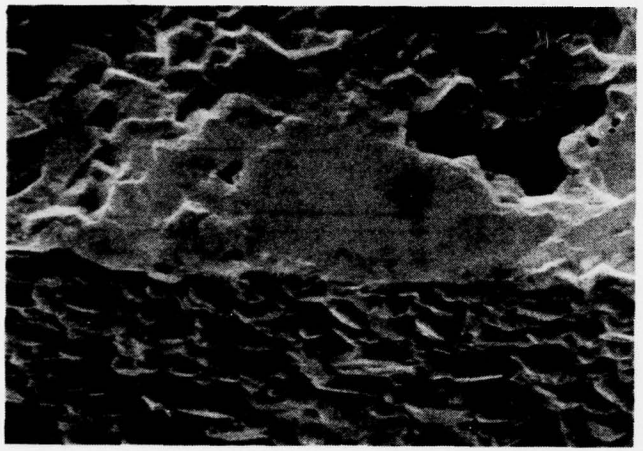

1000x 20μ

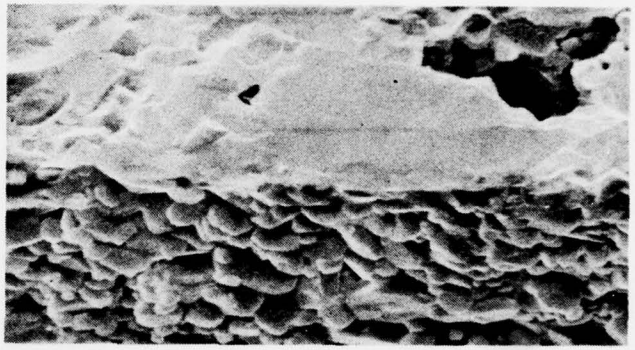

1000x 20μ

Figure 3 Fracture surface and thermally etched specimen surface of 96% alumina, stereo pair (Specimen E-4, 1000x).

has shown that, in a coarse grained alumina*, twins tend to propagate from one grain to the next and that microcracks initiate at the twins. Furthermore, he has shown that the twinning is a time consuming process that, based on a very long extrapolation of acoustic emission data, will be suppressed at strain rates of 10^8 sec^{-1}. Therefore, twinning is a possible mechanism by which transgranular fracture might spread from grain to grain but with decreasing frequency as the crack accelerates.

Subcritical crack growth at pores

Stereo SEM was used to examine fracture surfaces surrounding pores. An example, specimen N-37 fractured in flexure at -196°C, is shown in Figure 4. The fracture originated at the large pore near the center of the photo as indicated clearly by lines radiating from the pore. The pore is surrounded by a region of transgranular fracture. The straight edges under the pore indicate that at least part of the pore was bounded by a large grain but it is clear that the area of transgranular fracture spreads into other grains. It has been argued that the fracture stresses at pores can be calculated by assuming that the pore is surrounded by a crack one average grain size in depth. These arguments have been reviewed in detail by Rice[4]. In the present case one can estimate the critical flaw size assuming a penny-shaped crack, using Equation (1). The resulting flaw radius is 43 μm. This radius is clearly much larger than the radius of the pore plus one average grain size and it is also larger than the distance from the center of the pore to the straight boundary below the pore. Therefore, it is clear that in the present case, no simple rule

*LUCALOX, General Electric Company.

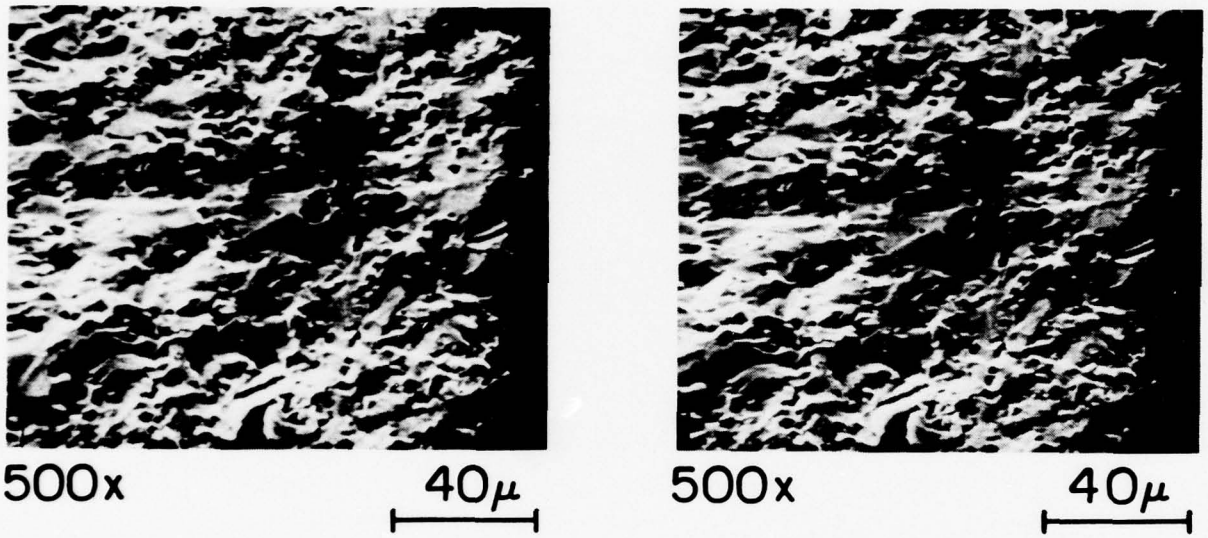

Figure 4 Fracture origin at a pore in 96% alumina stereopair, (specimen N-37 fractured at -196°C, 500x).

such as use of the radius of the pore plus one average grain size can be applied.

Further examination of the fracture surface reveals that many of the other pores, perhaps all of them, are surrounded by similar regions of transgranular fracture. This observation raises the question whether this transgranular fracture occurs as the crack front sweeps past the pores during fast fracture or, alternatively, whether it has occurred by subcritical crack growth before fast fracture begins at the fracture origin. If this transgranular fracture had occurred as the crack front swept past the pore, one might expect the regions before the crack reaches the pore (the near side) to be a combination of intergranular and transgranular fracture like the surrounding fracture surface and to observe transgranular fracture mainly on the far side of the pore. Examination of the regions surrounding pores shows that this is not the case. Therefore, the present evidence suggests that subcritical crack growth occurred at most of the pores as the specimen was loaded.

B. Relationships between stress intensity factor and percent intergranular fracture

Curves of stress intensity factor (K_I) vs. percent intergranular fracture (PIF) were plotted. Two distinct types of curves were observed. One type was very similar to those obtained for fine grained H.P. alumina[8], showing significant maxima and minima in PIF at various values of K_I. An example, for a specimen fractured in flexure at room temperature, is given in Figure 5. The surface flaw propagated as an

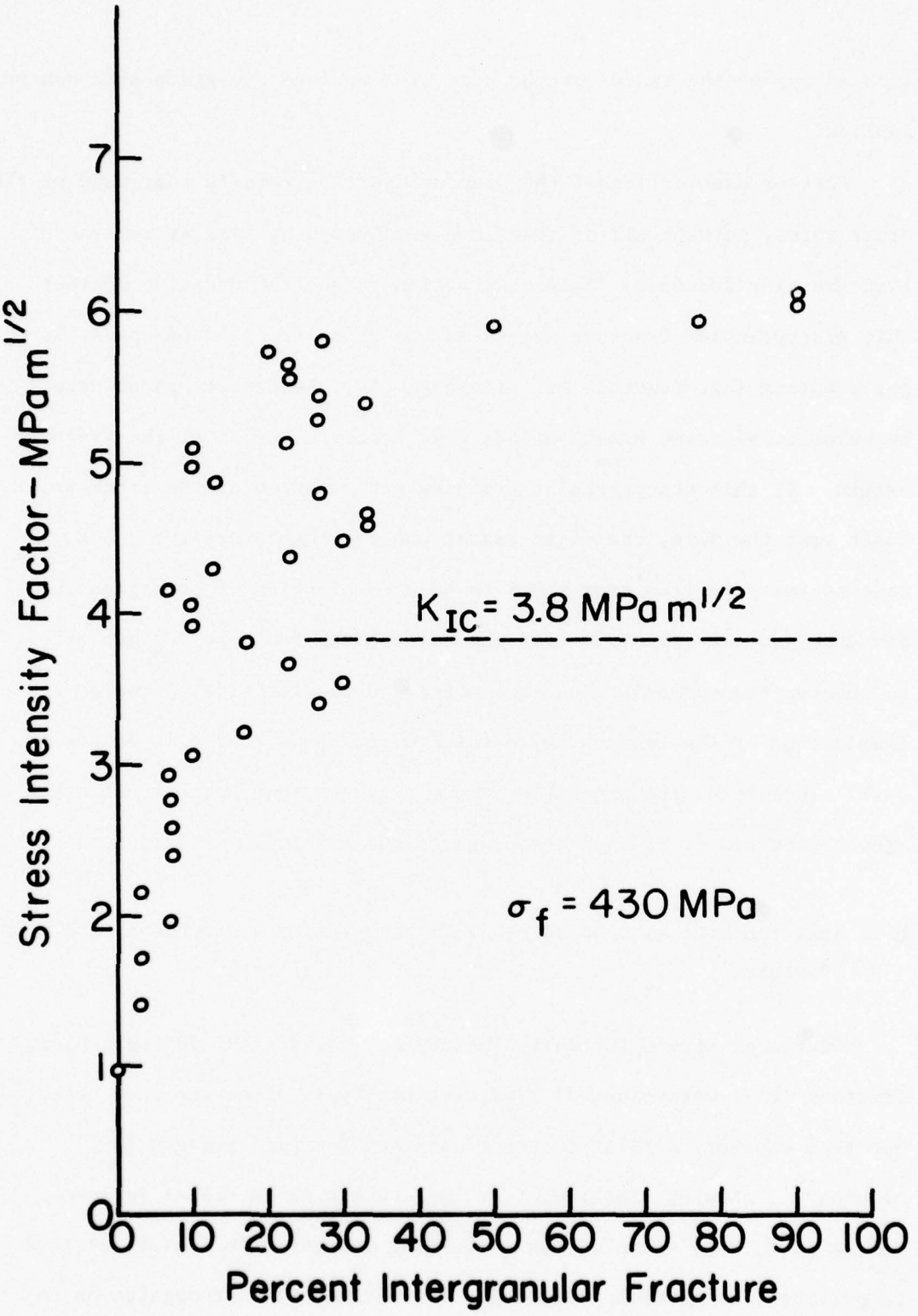

Figure 5 Stress Intensity Factor vs. Percent Intergranular Fracture; 96% Alumina (Specimen R-4 fractured in flexure at room temperature).

approximately semi-circular surface crack. As in the case of H.P. alumina, there is a rough correspondence between the values of K_I at the minima in PIF and the values of K_{IC} for fracture in various crystallographic directions in sapphire which were calculated using fracture energies measured by Wiederhorn[14,15] and listed in Table I. In particular, the minimum at about 4.1 $MPam^{1/2}$ is close to K_{IC} = 4.3 $MPam^{1/2}$ for the $\{\bar{1}\bar{1}26\}$ fracture plane and the minima at 5.1 and 5.7 $MPam^{1/2}$ are close to K_{IC} = 5.6 $MPam^{1/2}$ which, based on Wiederhorn's observations, is the value at which the fracture alternates between $\{\bar{1}012\}$ rhombohedral surfaces and chonchoidal surfaces roughly parallel to $\{01\bar{1}4\}$ planes. At K_I > 5.7 $MPam^{1/2}$ there is a strong trend toward intergranular fracture. K_{IC} for nominally the same 96% Al_2O_3 was measured by Bansal and Duckworth[16] yielding 3.8 $MPam^{1/2}$. Thus, the location of the minimum at K_I = 4.1 $MPam^{1/2}$ corresponds approximately with the location at which $K_I = K_{IC}$ for the polycrystalline material as observed for H.P. alumina.

Two views of the fracture surface of this specimen are given in Figure 6. Figure 6A is a general view of the fracture surface showing the flaw at the fracture origin surrounded by a darker region. At higher magnification in Figure 6B, the darker region is clearly shown to be a region of transgranular fracture. This region is bounded by a region that is much rougher and more varied in appearance. Voids of various irregular shapes and sizes form a rough semicircle at the boundary. Also, there are a substantial number of individual grains, fractured intergranularly, projecting above the average level of the surface just outside this boundary. The coexistence of these features suggests that many of the

Table I. Fracture Energies[14,15] and Critical Stress Intensity Factors for Several Crystal Lattice Planes in Sapphire.

Fracture Plane	Fracture Energy Jm^{-2}	Critical Stress Intensity Factor $MPam^{1/2}$
$\bar{1}012$	6.0	2.15 (1.7)*
$10\bar{1}0$	7.3	2.4
$\bar{1}\bar{1}26$	24.4	4.3
0001	>40	>5.6

*See reference 15.

A. Fracture surface (30x)

B. Fracture origin (500x)

Figure 6 Fracture surface and fracture origin in 96% alumina (Specimen R-4, fractured at room temperature at 430 MPa).

voids are the result of pullouts of the intergranularly fractured grains. The flaw radius at this boundary is 50 μm which corresponds to K_I = 3.9 $MPam^{1/2}$, a value very close to K_{IC} of the polycrystalline material.

Somewhat similar results were obtained for a specimen fractured in flexure at -196°C. At this temperature, the strength of 96% alumina is much greater than it is at room temperature and the material is much less susceptible to surface flaw failure[5,9]. Fracture in this particular specimen which is the same as that illustrated previously in Figures 2 and 4, originated at a pore located about 60 μm from the surface at a stress of 623 MPa. Near the origin the fracture is primarily transgranular. The K_I vs. PIF curve is given in Figure 7. The fracture surface has such a high degree of transgranularity that opportunities for the minima to manifest themselves are limited. There is an increase in PIF at K_I values above 4 $MPam^{1/2}$, followed by a decrease to 0% PIF at 4.9 $MPam^{1/2}$. Above K_I = 6 $MPam^{1/2}$ there is a strong trend toward increasing PIF as there was in the previous case.

One cannot make a definite comparison between the variations in PIF and K_{IC} of the polycrystalline material because K_{IC} has not been measured for this material at -196°C. If one assumes that the fracture mechanisms at the critical crack growth boundary and at crack branching vary the same way at -196°C as they do at room temperature, one can estimate K_{IC} at -196°C from the slopes of fracture stress -(mirror radius)$^{-1/2}$ curves which are proportional to the stress intensity factors at crack branching. These slopes are 8.3 $MPam^{1/2}$ at room temperature and 10.0 $MPam^{1/2}$ at -196°C[17].

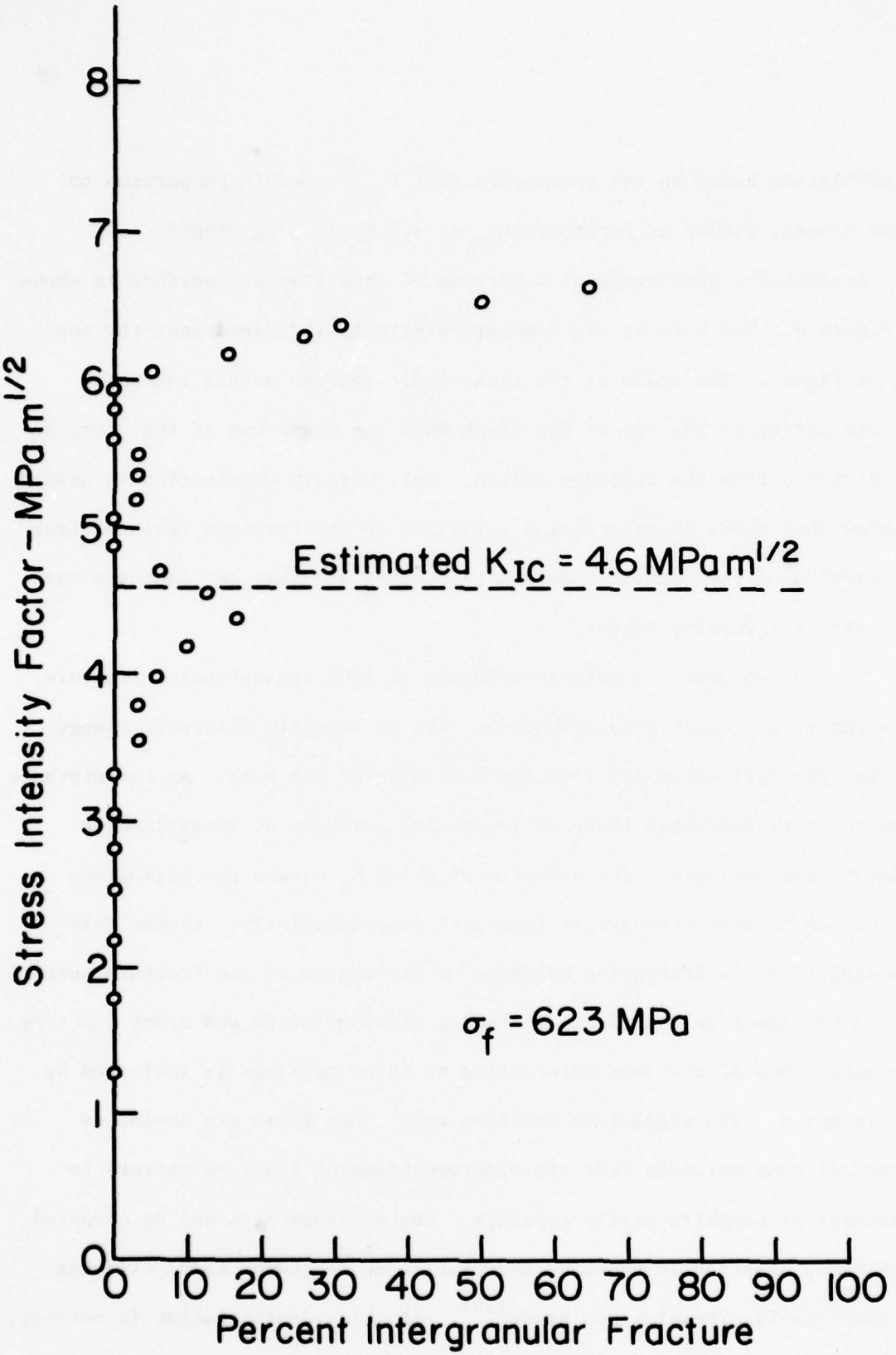

Figure 7 Stress Intensity Factor vs. Percent Intergranular Fracture in 96% Al_2O_3 (Specimen N-37 fractured in flexure at −196°C).

A calculation based on the assumption that K_{IC} varies in proportion to these slopes, yields an estimated K_{IC} of 4.6 $MPam^{1/2}$ at -196°C.

A composite photograph of a portion of this fracture surface is shown in Figure 8. The pore at the fracture origin is indicated near the top of the figure. The scale at the right indicates the stress intensity factors acting at the tip of the crack when the crack was at that particular distance from the fracture origin. Only cursory examination is needed to show that there is substantial variation in the fracture features from one portion of the fracture surface to another and that the features vary with stress intensity factor.

The region near the pore is a region of 100% transgranular fracture. Apparently, the crack grew around the pore on slightly different planes forming the tail extending from the left side of the pore. As the distance from the pore increased there is increasing evidence of intergranular fracture and pullouts. The boundary at which K_I equals the estimated K_{IC} passes through some grains fractured intergranularly. Beyond this boundary there is increasing evidence of disruption of the fracture surface caused by higher values of K_I, including cleavage steps and other fracture markings. One of the most interesting of these markings is indicated by the letter A. The suggestion has been made* that these are so-called cathedral dome markings that are observed bounding fracture mirrors in fractures of sapphire single crystals. The markings at A can be compared with those observed in sapphire and attributed to rhombohedral cleavage by Abdel-Latif, Tressler and Bradt[18]. If this identification is correct,

---

*By R. W. Rice, Naval Research Laboratory.

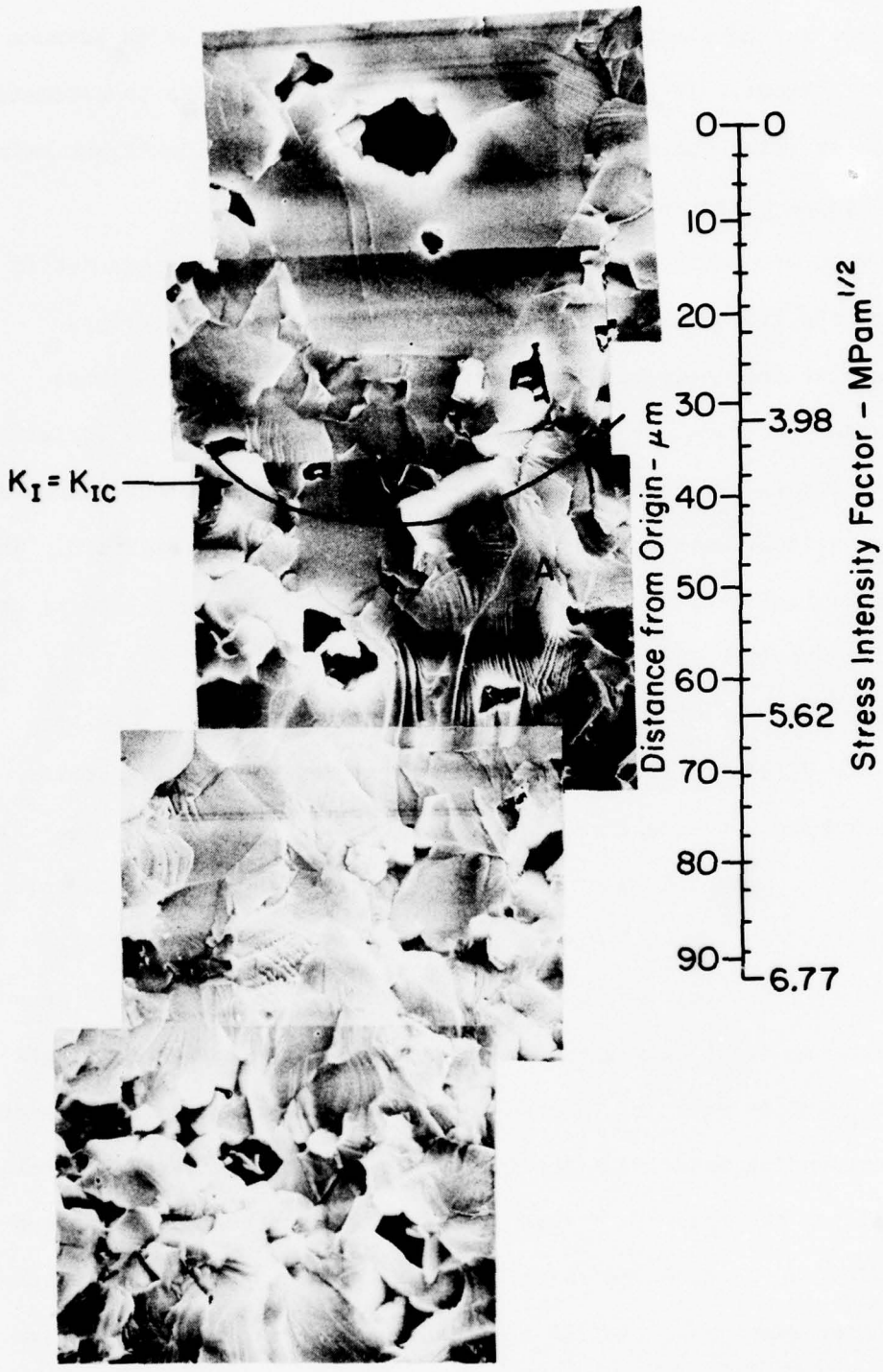

Figure 8 Composite photograph of the fracture surface along a radius from the fracture origin in 96 % alumina (Specimen N-37, fractured at -196 °C).

the features may have arisen as a result of crack formation in advance of the crack front. If that is the case it may be possible to estimate the stress at which the crack formed in advance of the crack front using fracture stress-mirror size relations[3,17,19].

The fracture energy at a particular stage of crack propagation is the sum of the fracture energies of the individual fracture events (transgranular and intergranular fracture on various lattice planes, microplastic processes, etc.). These processes have extremely variable fracture energies as shown in Table I. The frequencies of the processes vary substantially with K_I and crack velocity as shown in Figure 8. Therefore, substantial variations in fracture energy at various stages of crack propagation should be expected.

The second type of K_I vs. PIF curve is given in Figure 9 for a specimen fractured in flexure at room temperature. This curve bears little resemblance to the curves obtained for H.P. alumina[8]. The fracture is transgranular near the fracture origin but above some value of K_I, in this case about 3 $MPam^{1/2}$, there is a gradual trend toward intergranular fracture. It is suggested that this second type of curve occurs when the crack propagation goes critical with respect to single crystal K_{IC} values near the fracture origin and the crack is not arrested by the surrounding material. The importance of single crystal K_{IC} values in determining the fracture stress of coarse grained ceramics has been emphasized by R. W. Rice and co-workers[20]. If the present explanation is correct it means that the 96% alumina is a material having relative flaw sizes and grain sizes in a transition range. It would be reasonable

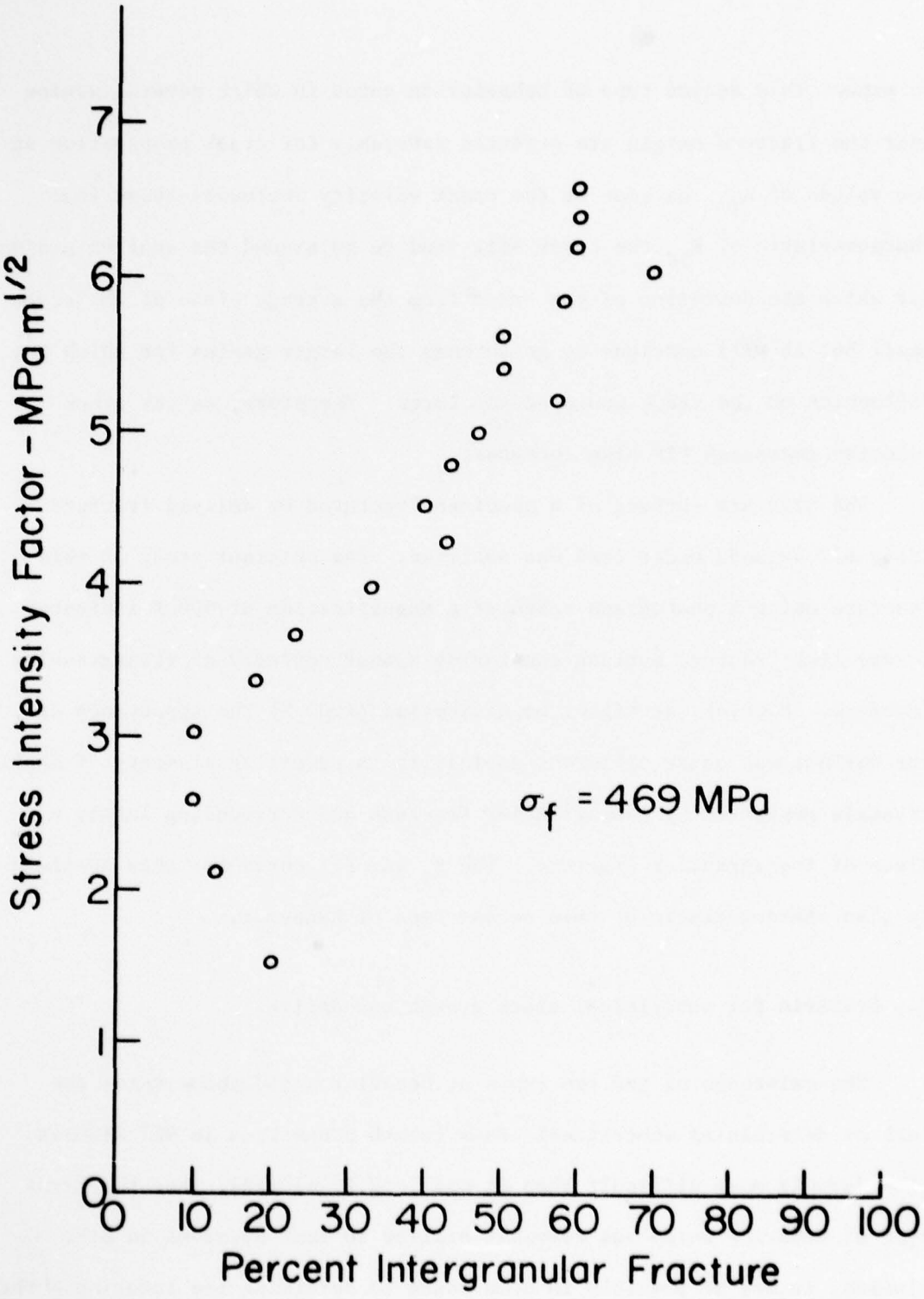

Figure 9 Stress Intensity Factor vs. Percent Intergranular Fracture (Specimen R-11, fractured in flexure at room temperature).

to expect this second type of behavior in cases in which several grains near the fracture origin are oriented favorably for crack propagation at low values of K_I. As soon as the crack velocity increases above that characteristic of K_{IC} the crack will tend to go around the smaller grains for which the deviation of the crack from the average plane of the crack is small but it will continue to go through the larger grains for which the deflection of the crack would be too large. Therefore, as the crack velocity increases PIF also increases.

The fracture surface of a specimen fractured by delayed fracture after 622 seconds under load was analyzed. The original study of this fracture using a photograph taken at a magnification of 600 X indicated a very flat fracture surface consisting almost entirely of transgranular fracture. However, at higher magnification (1000 X) the appearance of the surface was quite different especially in revealing clusters of small crystals separated by intergranular fracture and surrounding larger areas of transgranular fracture. The K_I vs. PIF curve for this specimen is also characteristic of this second type of behavior.

C. Criteria for subcritical crack growth boundaries

The existence of the two types of behavior noted above makes the task of determining subcritical crack growth boundaries in 96% alumina considerably more difficult than it was in H.P. alumina. For the first type of behavior which was somewhat similar to that observed in H.P. alumina, it may be possible in some cases to determine the location of the minimum in PIF near $K_I = 4$ MPam$^{1/2}$ and use this boundary as the subcritical

crack growth boundary. In other cases there may be very little intergranular fracture so this minimum may be poorly defined. In those cases it may be possible to use the boundary determined by isolated projecting grains (intergranularly fractured grains) from the fracture surface as illustrated by Figures 8 and 10. In Figure 10 the projecting grains seem to be of average size whereas those in Figure 8 and the one illustrated by Bansal and Duckworth[7] were larger than average size.

As a means of confirming the location of the subcritical crack growth boundary for the first type of behavior, one can locate the boundary formed by the onset of cleavage steps and other signs of severe disturbance in a substantial fraction of grains. This boundary falls at a greater distance from the fracture origin than that of the subcritical crack growth boundary. Therefore, by comparing the locations of various alternative subcritical crack growth boundaries with this boundary formed by the onset of cleavage steps, one may be able to make a more reliable decision.

Locating the subcritical crack growth boundary for the second type of behavior is more difficult. No particular fracture features were noted at low values of stress intensity factor. Therefore, the best procedure seems to be to consider the stress intensity factor, at which the long trend toward increasing K_I begins, as the critical stress intensity factor at this boundary. The crack depth to this boundary can be calculated using Equation (1) making it possible to locate the boundary.

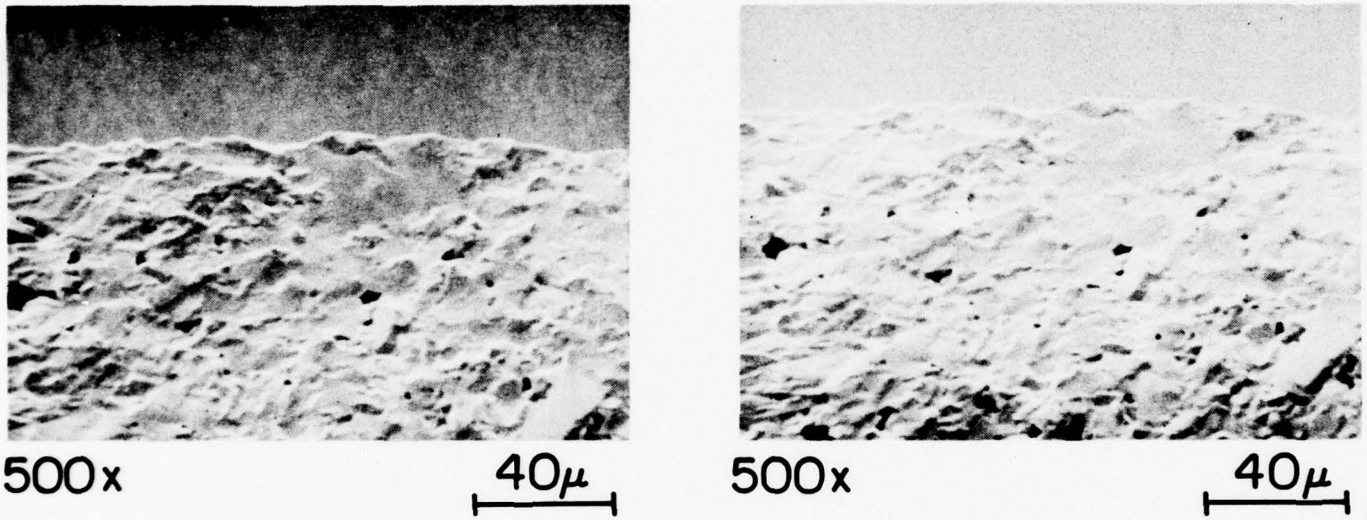

Figure 10 Fracture surface of a 96% alumina specimen fractured at room temperature stereopair,(Specimen R-8, fracture stress 457 MPa) mag.

IV. Conclusions

As in the case of H.P. alumina, K_I vs. PIF curves can be used to determine criteria for locating subcritical crack growth boundaries in 96% alumina. Two types of curves were observed. The first of these types seems to be similar in most respects to curves plotted for H.P. alumina. 96% alumina has a greater tendency to fracture transgranularly near fracture origins, compared with H.P. alumina. This tendency may be a result of the larger grain size. The fact that fractures around the grains (intergranular fracture) require greater deviations from the main fracture plane; and that such deviations would require more energy, favors transgranular fracture. As in H.P. alumina, the subcritical crack growth boundaries of 96% alumina specimens characterized by the first type of curve, can be located using the minimum in the K_I vs. PIF curve near $K_I = 4\ MPam^{1/2}$. If there is so little intergranular fracture that the minima do not have an opportunity to manifest themselves, the boundary can be located at the boundary indicated by isolated grains projecting from the fracture surface.

The second type of curve is characterized by a trend toward higher PIF beginning at much lower K_I (near $K_I = 3\ MPam^{1/2}$). It is suggested that this type of curve may be observed in cases in which the crack front accelerates to high velocities while it is propagating at K_I values slightly above the K_{IC} values for fracture on particular lattice planes of the individual crystals. As the crack accelerates there is insufficient time for transgranular fracture to occur in an increasing fraction

of cases so that there is a gradual increase in PIF. If this interpretation is correct, it indicates that the 96% alumina is a transition material, as far as grain size is concerned. In other words, in some cases the crack propagation goes critical at K_{IC} values characteristic of a fine grained polycrystalline material and in other cases it goes critical at lower values of K_{IC} just above the values measured for fracture on individual lattice planes that fracture at relatively low fracture energies.

Acknowledgments

The authors are pleased to acknowledge the contributions of their associates at Ceramic Finishing Company, helpful discussions with R. W. Rice, J. J. Mecholsky and P. F. Becker at the Naval Research Laboratory and Professor R. E. Tressler at The Pennsylvania State University, and the sponsorship of the Naval Air Systems Command.

References

1. H. P. Kirchner, W. R. Buessem, R. M. Gruver, D. R. Platts, and Ralph E. Walker, "Chemical Strengthening of Ceramic Materials," Ceramic Finishing Company Summary Report, Contract N00019-70-C-0418 (December, 1970).

2. A. G. Evans and G. Tappin, "Effects of Microstructure on the Stress to Propagate Inherent Flaws," Proc. Brit. Ceram. Soc. 20, 275-297 (June, 1972).

3. H. P. Kirchner and R. M. Gruver, "Fracture Mirrors in Alumina Ceramics," Phil. Mag. 27 (6) 1433-1446 (June, 1973).

4. R. W. Rice, "Fractographic Identification of Strength Controlling Flaws and Microstructure," from Fracture Mechanics of Ceramics, Vol. 1, Edited by R. C. Bradt, D. P. H. Hasselman and F. F. Lange, Plenum, New York (1974), pages 323-345.

5. R. M. Gruver, W. A. Sotter and H. P. Kirchner, "Variation of Fracture Stress with Flaw Character in 96% Al_2O_3," Bull. Amer. Ceram. Soc. 55 (2) 198-202 (February, 1976).

6. H. P. Kirchner, R. M. Gruver and W. A. Sotter, "Characteristics of Flaws at Fracture Origins and Fracture Stress-Flaw Size Relations in Various Ceramics," Mater. Sci. Eng. 22, 147-156 (1976).

7. G. K. Bansal, W. H. Duckworth and D. E. Niesg, "Strength-Size Relations in Ceramic Materials: Investigation of an Alumina Ceramic," J. Amer. Ceram. Soc. 59 (11-12) 472-478 (1976).

8. H. P. Kirchner and R. M. Gruver, "A Fractographic Criterion for Subcritical Crack Growth Boundaries in Hot Pressed Alumina," Submitted for publication.

9. R. M. Gruver, W. A. Sotter and H. P. Kirchner, "Fractography of Ceramics," Ceramic Finishing Company Summary Report, Contract N00019-73-C-0356 (November, 1974).

10. P. F. Becher, "Fracture Strength Anisotropy of Sapphire," J. Amer. Ceram. Soc. 59 (1-2) 59-61 (1976).

11. J. Lankford, "Compressive Strength and Microplasticity in Polycrystalline Alumina," J. Mater. Sci. 12, 791-796 (1977).

12. J. Lankford, Jr., "Tensile Failure of Unflawed Polycrystalline Alumina," J. Mater. Sci. 13, 351-357 (1978).

13. J. Lankford, Jr., "Compressive Microfracture and Indentation Damage in Alumina," from Fracture Mechanics of Ceramics, Vol. 3, Edited by R. C. Bradt, D. P. H. Hasselman, and F. F. Lange, Plenum, New York (1978), p. 245-255.

14. S. M. Wiederhorn, "Fracture of Sapphire," J. Amer. Ceram. Soc. 52 (9) 485-491 (1969).

15. S. M. Wiederhorn, "Subcritical Crack Growth in Ceramics," from Fracture Mechanics of Ceramics, Vol. 2, Edited by R. C. Bradt, D. P. H. Hasselman and F. F. Lange, Plenum, New York (1974), p. 190.

16. G. K. Bansal and W. H. Duckworth, "Effect of Specimen Size on Ceramic Strengths," from Fracture Mechanics of Ceramics, Vol. 3, Edited by R. C. Bradt, D. P. H. Hasselman and F. F. Lange, Plenum, New York (1978), pp. 189-204.

17. H. P. Kirchner, R. M. Gruver, W. A. Sotter, "The Variation of Fracture Mirror Radius with Fracture Stress for Polycrystalline Ceramics under Various Loading Conditions," Ceramic Finishing Company Technical Report No. 2, Contract N00014-74-C-0241 (1974).

18. A. I. A. Abdel-Latif, R. E. Tressler and R. C. Bradt, "Fracture Mirror Formation in Single Crystal Alumina," from Fracture 1977, Vol. 3, Edited by D. M. R. Tappin, University of Waterloo Press, Waterloo, Ontario (1977), pp. 933-939.

19. H. P. Kirchner, "The Strain Intensity Criterion for Crack Branching in Ceramics," Eng. Fracture Mechanics 10, 283-288 (1978).

20. R. W. Rice, "Microstructure Dependence of Mechanical Behavior of Ceramics," from Treatise on Materials Science and Technology, Vol. II, Academic Press, New York (1977).

A Fractographic Criterion for Subcritical Crack Growth Boundaries at Internal Fracture Origins in Hot Pressed Silicon Nitride

by

H. P. Kirchner

R. M. Gruver

D. M. Richard

Ceramic Finishing Company
P.O. Box 498
State College, PA 16801

Abstract

Using the elliptic integral method, stress intensity factors (K_I) were estimated at boundaries defined by fracture features observed at various distances from internal fracture origins in H.P. silicon nitride. The fracture origins are surrounded by regions of transgranular fracture. At the outer boundaries of these regions K_I is less than K_{IC} showing that these are regions of subcritical crack growth. Regions of hummocks and depressions were observed surrounding the regions of transgranular fracture. K_I was calculated at the elliptical boundary determined by the outer edge of the nearest of these features to the fracture origin. At this boundary, $K_I \tilde{=} K_{IC}$. Therefore, these features can be used to locate the subcritical crack growth boundary.

I. Introduction

Development of fracture theories and methods of failure analysis has been handicapped by the lack of fractographic criteria for locating subcritical crack growth boundaries in fracture surfaces of ceramics. In this paper such a criterion is described for a particular hot pressed (H.P.) silicon nitride ceramic.

Fracture origins in H.P. silicon nitride, fractured at room temperature, are easily located in most cases at the intersection of the extensions of lines drawn through the hackle. In some cases other types of lines oriented in the direction of the fracture origin can be observed in the fracture surface. Because the material is strong and fine grained, these fracture features are well defined, aiding in location of the fracture origins. Although individual grains in fracture surfaces may strongly reflect incident light, the areas of reflecting spots that are so helpful in locating fracture origins in alumina ceramics are not observed in H.P. silicon nitride.

Flaws at fracture origins in H.P. silicon nitride specimens, fractured at various temperatures and loading rates, were located and characterized by Kirchner, Gruver and Sotter[1,2] and Baratta, Driscoll and Katz[3]. Recently, D. G. Miller et al.[4] described a number of such flaws. At room temperature, fracture may originate at various types of flaws including machining damage, pores, large crystals and inclusions. However, with improved surface finish and increased volume under stress (tensile tests or large specimens) there is increased tendency for fracture

to originate at internal flaws, frequently inclusions associated with pores. The fracture stress increases with increasing transformation of alpha to beta silicon nitride[5,6]. This increase has been attributed to increased particle elongation.

Attempts to measure the variation of crack velocity with stress intensity factor (K_I) at room temperature using standard techniques such as the double torsion beam test have, thus far, not been successful. Apparently, crack velocity increases so rapidly with K_I that it has not been possible to achieve stable crack propagation. However, there is a small slow crack growth effect in H.P. silicon nitride[1]. Twenty cylindrical rods were loaded in flexure to a constant stress of 629 MPa in air at 18-22% relative humidity. Four of the specimens fractured on loading (< 1 s) and seven survived for more than 1000 s after which the test was terminated. The remaining specimens (9) fractured after various times ranging from one to 863 s. Results consistent with these observations were obtained by Gulden and Metcalfe[7]. They observed a substantial stress corrosion effect but 10% of the fractures originated at internal flaws to which the test environment did not have direct access perhaps showing that a corrosive environment is not necessary for slow crack growth to occur in this material.

Evans and Tappin[8] and Bansal, Duckworth and Niesz[9,10] have attempted to locate critical flaw boundaries after subcritical crack growth and flaw linking in several ceramics. However, as indicated by Rice[11], considerable subjective judgement is involved in such attempts. It would be desirable to have more objective criteria for locating these boundaries. Kirchner and Gruver[12,13] have used the variation of the

percent intergranular fracture (PIF) with K_I to develop such criteria for H.P. alumina and 96% alumina. In the present investigation, this technique was used to develop a criterion for locating subcritical crack growth boundaries in silicon nitride.

II. Procedures

The present research was done by fractographic analysis of H.P. silicon nitride specimens* fractured in tension in an earlier investigation. Preparation and testing of these specimens was described previously[1,7]. The specimens were cylindrical rods necked down to form a test section about 1.4 mm diameter. The loading rate was rather slow, requiring more than one minute to fracture the specimens. The fracture surfaces were studied by optical and scanning electron microscopy (SEM) including stereo SEM.

The fractures originated at internal flaws which were surrounded by regions of transgranular fracture. Two principal methods of analysis were used. The first method involved outlining the outer boundary of the region of transgranular fracture and using the elliptic integral method[14] to calculate the stress intensity factors at the intersections of the major and minor axes with this boundary. The stress intensity factor (K_I) was calculated using

$$K_I = \frac{Y\sigma}{\Phi}\left(\frac{a}{c}\right)^{1/2}\left(a^2\cos^2\theta + c^2\sin^2\theta\right)^{1/4} \qquad (1)$$

in which a, c and θ are defined by

*NC-132, Norton Company, Worcester, MA.

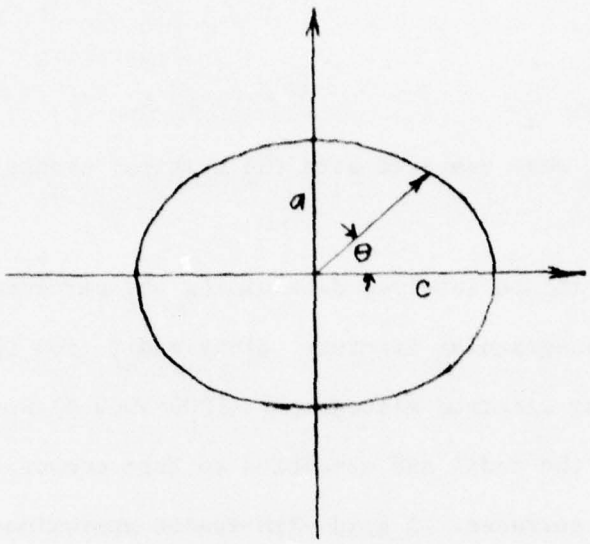

That is, a is 1/2 the minor axis of the ellipse, c is 1/2 the major axis of the ellipse, and θ is the angle between the major axis and a radius of the ellipse. Φ is defined by the following integral

$$\Phi = \int_0^{\frac{\pi}{2}} \left[1 - \left(1 - \frac{a^2}{c^2}\right) \sin^2\theta\right]^{1/2} d\theta \qquad (2)$$

which is an elliptic integral of the second kind. Mathematical tables were used to determine the values of this integral. To determine K_I at the intersection of the minor axes with the boundary of the ellipse, θ is taken as $\frac{\pi}{2}$ in Equation (1) yielding

$$K_{I_{max}} \left(\theta = \frac{\pi}{2}\right) = \frac{Y \sigma}{\Phi} a^{1/2} \qquad (3)$$

Similarly, for the intersection with the major axis

$$K_{I_{min}} (\theta = 0) = \frac{Y \sigma}{\Phi} a^{1/2} \left(\frac{a}{c}\right)^{1/2} \qquad (4)$$

The values of K_I were compared with the critical stress intensity factor (K_{IC}).

The second method involved determining the percentages of intergranular and transgranular fracture along radii from the fracture origin. Scanning electron micrographs (1000-5000 X) were taken at intervals along the radii and assembled to form composite photographs of the fracture surfaces. A grid with spaces approximately equal to one grain size and ten spaces wide was prepared. The grid was placed on the composite photograph and the fracture surface at the center of each grid space was examined and classified as to whether it was intergranular or transgranular, characterizing a path about ten grains wide. This process was repeated for adjoining rows of the grid. The percentages of intergranular and transgranular fracture varied considerably from one row to the next so averages were calculated for each row which included the results of the preceding and following rows to form three row running averages. The percentages of intergranular fracture (PIF) were plotted vs. the stress intensity factors calculated at the various points along the radii when the crack front was at each point. The calculations of K_I were done using the fracture stress so that the results are strictly correct only for delayed fracture (constant load) specimens for which the applied stress is constant. For specimens fractured by a linearly increasing load, the K_I values are overestimated at all crack lengths except the critical crack length because the stress is overestimated. However, calculations show that almost all of the crack growth occurs in less than the last 10% of the loading time. In this time the applied stress varies by less than 10%. Therefore, the error in the calculated K_I values is small for most of the crack growth.

III. Results and Discussion

General observations

Most of the results of this investigation were obtained from five specimens fractured in uniform tension. All of the fractures originated at what appeared to be inclusions, pores or porous regions (Figure 1). The flaws at the fracture origins ranged in size from the average grain size (1-2 μm) to several times that size. When the fracture surfaces were rotated in the SEM, it was observed that, in particular orientations, each fracture origin was surrounded by a rather dark elliptical region (Figure 2). Such a dark region was observed previously by Baratta et al.[3]. At slightly higher magnification it was observed that these regions contained a large fraction of transgranularly fractured grains (Figure 3).

Outside the dark elliptical region is a region in which the surface is more uneven, as indicated by light and dark blotches. At higher magnification using stereo SEM these blotches are observed to be hummocks and depressions which form a wide band outside the dark elliptical region.

Numerous pores are observed in the wide band of hummocks and depressions. Many of these pores are surrounded by small regions of transgranular fracture. These observations are additional evidence of the tendency of cracks originating at pores to grow by subcritical crack growth.

Stress intensity factors at boundaries of dark elliptical regions

The elliptic integral method was used to calculate values of K_I at the intersections of the major and minor axes with the boundaries of these

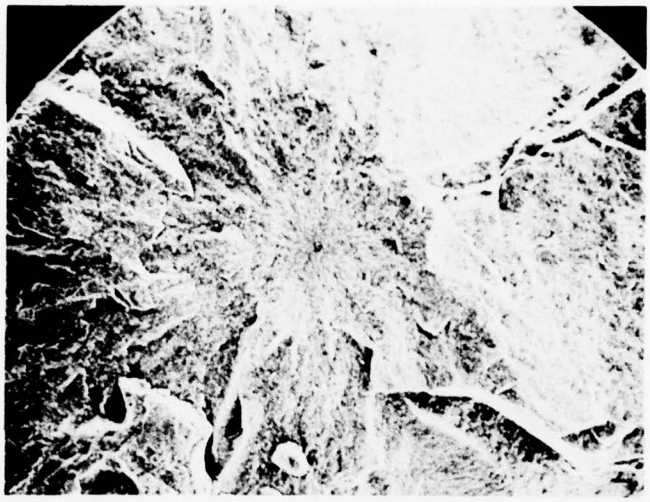

A. Fracture surface (70X)

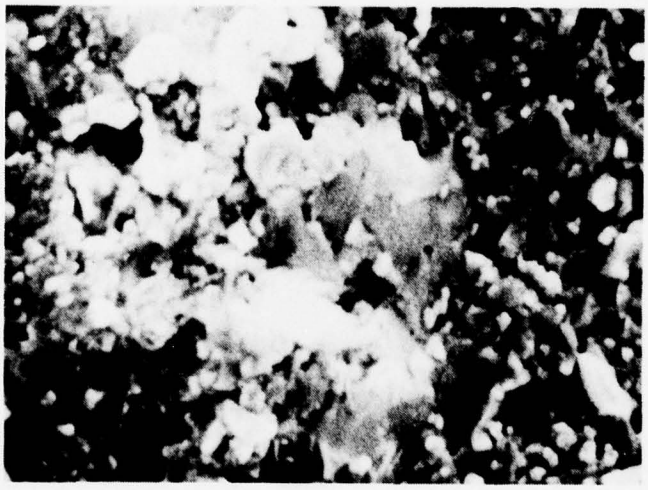

B. Fracture origin (7000X)

2 μm

Figure 1 Fracture surface and internal fracture origin, specimen 2T

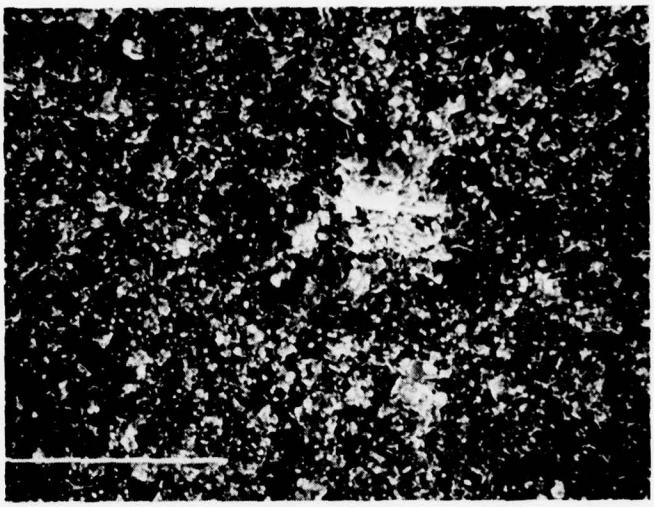

Figure 2 Dark region surrounding fracture origin, specimen 4T (1000X)

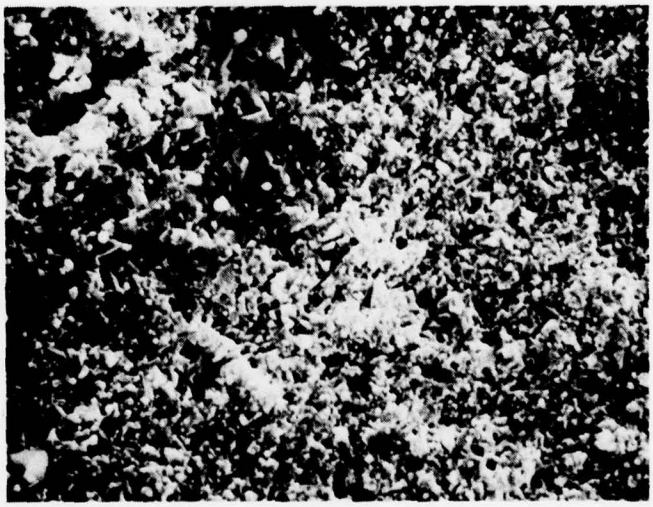

Figure 3 Transgranular fracture at fracture origin, specimen 1T (1500X)

ellipses yielding the results shown in Table I. As expected, the higher values of K_I occur at the intersections of the minor axes with the boundaries of the ellipses. These values range from 3.16 to 4.65 $MPam^{1/2}$. The highest value is slightly less than a widely accepted value of K_{IC} which is 4.7 $MPam^{1/2}$[15,16].

The K_I values in Table I seem to be too low to support the hypothesis that the subcritical crack growth boundary is the boundary of the dark region of grains fractured mainly by transgranular fracture. Therefore, the fracture surfaces were examined for other features that might serve to locate the subcritical crack growth boundary. Outside the boundary of the dark area are numerous features that might be described as hummocks and depressions as shown in the stereo pairs in Figures 4 and 5. Many of the hummocks and depressions are elongated radially from the fracture origin. These features are not hackle which are observed at much greater distances from the fracture origin. At low magnification the elongated hummocks and depressions give the fracture surface a somewhat fibrous appearance. The normal range of sizes of these features is about 4-8 μm.

Based on the above observations, it was hypothesized that the hummocks consisted of agglomerates that were resistant to fracture so that, for crack propagation to occur at the velocity characteristic of the particular K_I value, it is necessary for the crack to propagate around the agglomerates. Assuming this to be the case a rough boundary outside the first "row" of these hummocks and depressions was visualized and the minor axis was measured. The eccentricity of the ellipse was assumed to

Table I. Stress Intensity Factors* at the Boundaries of the Dark Ellipses in H.P. Si_3N_4 Specimens Fractured in Tension.

Spec. No.	Fracture Stress MPa	Minor Axis (a) μm	Major Axis (c) μm	Eccentricity (a/c)	Φ	Stress Intensity Factor $K_{I_{max}}$ $MPam^{1/2}$	Stress Intensity Factor $K_{I_{min}}$ $MPam^{1/2}$
1T	529	17	31	.55	1.242	3.16	2.34
2T	896	9	11	.82	1.432	3.38	3.06
3T	716	20	36.7	.54	1.240	4.65	3.42
4T	651	19	23	.83	1.437	3.55	3.23
5T	708	17.5	35	.50	1.211	4.40	3.11

*$K_{I_{max}} = \frac{Y \sigma_f (a)^{1/2}}{\Phi}$ where Y was taken as 1.8 for internal flaws.

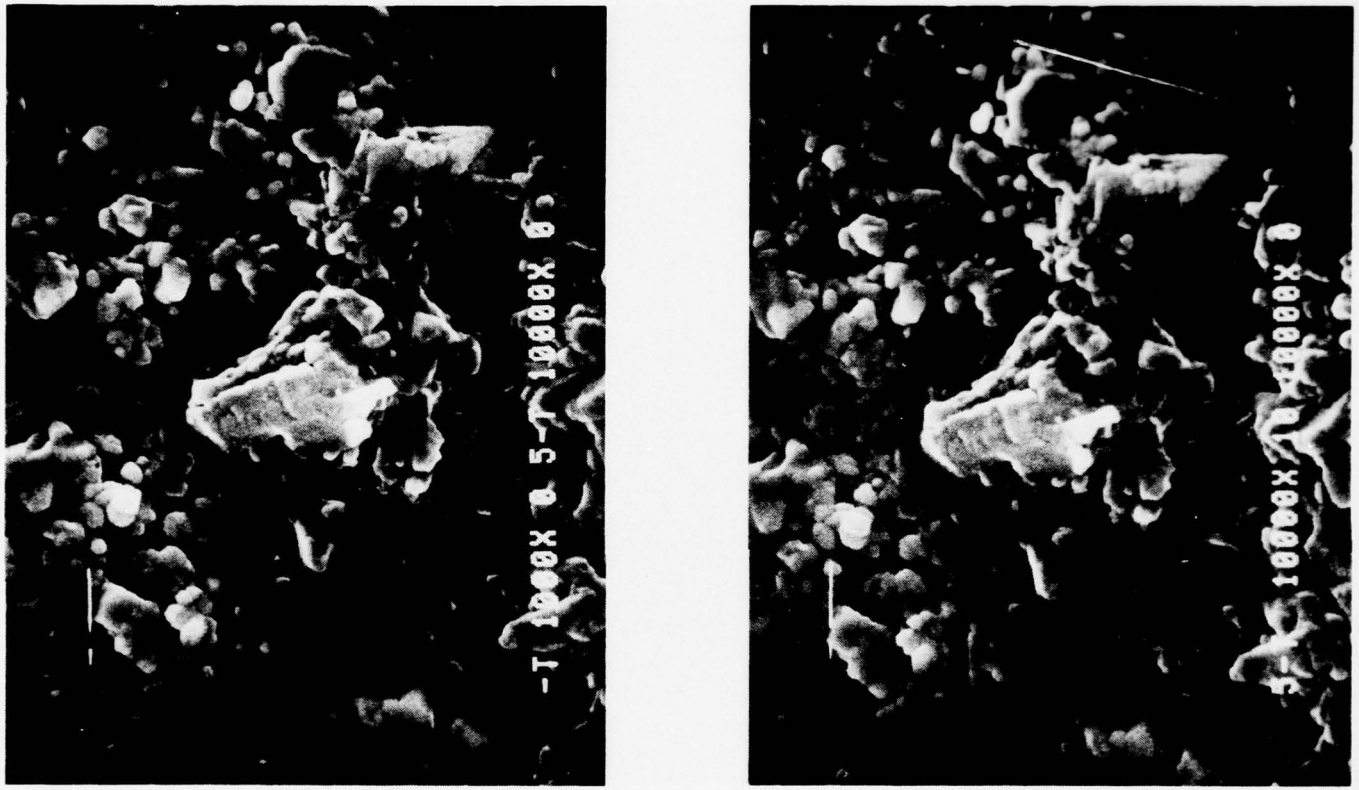

Figure 4 Hummock surrounded by depressions, specimen 5T, stereo pair (10,000X)

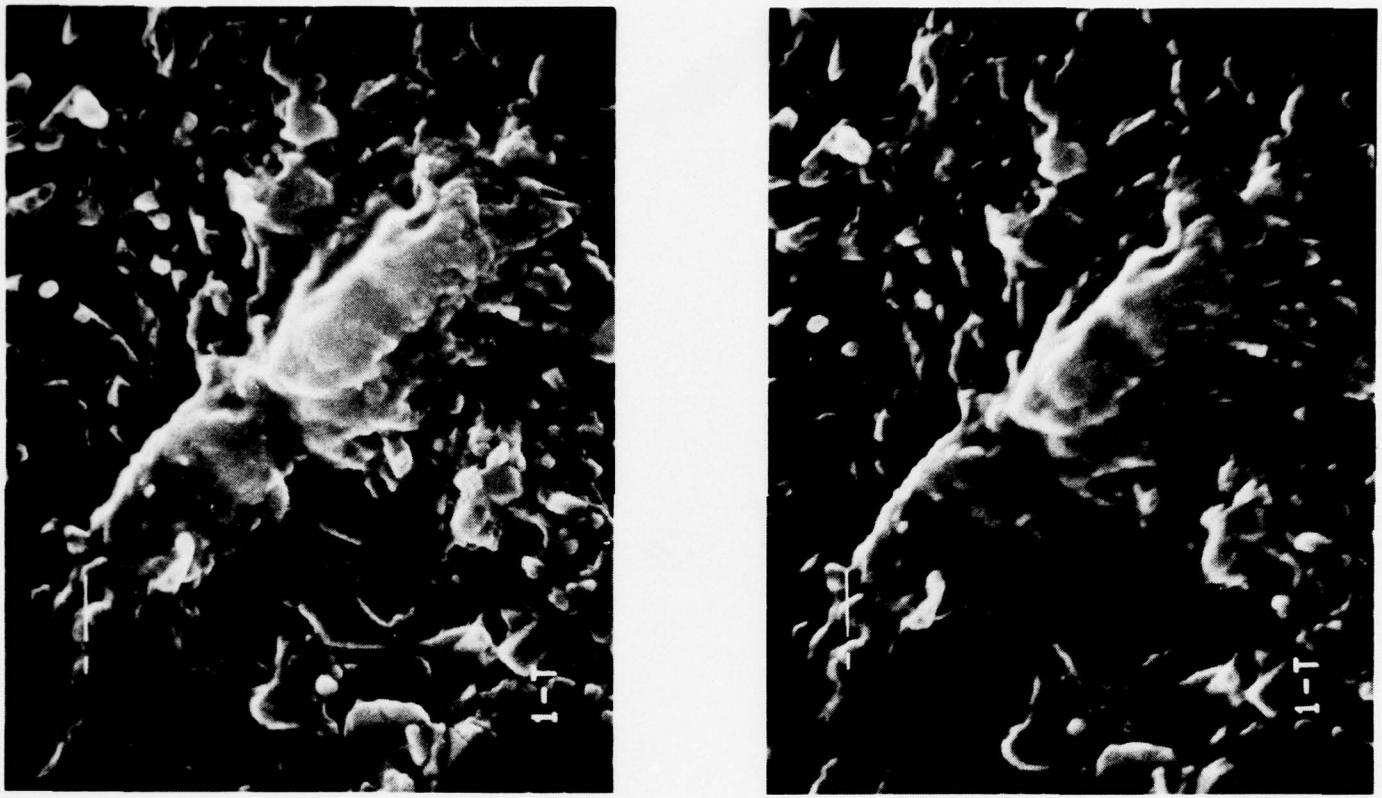

Figure 5 Hummock surrounded by depressions, specimen 1T, stereo pair (10,000X)

be the same as that of the dark region. The resulting K_I values are given in Table II. These values are more consistent with the measured K_{IC}.

The fact that these K_I values are somewhat scattered is not surprising because of experimental uncertainties in measurement of the ellipses and local variations in material properties such as K_{IC}. One expects fractures to originate in the regions that have the most vulnerable combination of flaw severity and reduced local K_{IC}.

The mechanism by which the agglomerates resist fracture was studied. An etched fracture photographed by Miller et al.[4] shows hummocks and depressions of the same size as those observed in the present investigation. The hummocks appear to contain elongated grains with preferred orientations tending to be perpendicular to the fracture surface. Therefore, the agglomerates may resist fracture because they consist of elongated grains with preferred orientations perpendicular to the crack front. The hummock illustrated in Figure 4 evidently resisted fracture because of the presence of the elongated grains at the "leading" edge of the hummock. In other cases such as Figure 5 similar grains were not observed but may have been present within the hummock. Figure 28 of Bowen[6], Figure 5, and some of the composite photographs not included because they are too large, show that the depressions contain many grains elongated parallel to the fracture surface. Interspersed among these grains are individual elongated grains that have either pulled out of the opposite surface of the crack or fractured through the grain. These observations are interpreted to mean that the crack propagates by transgranular fracture until it speeds up to the point that it no longer can pass through the hummocks by transgranular

Table II. Revised Stress Intensity Factors for Boundaries at the Far Side of Hummocks and Depressions Near Minor Axis of the Dark Ellipse.

Specimen Number	Fracture Stress MPa	Revised Minor Axis (a) μm	Φ	Revised $K_{I_{max}}$ $MPam^{1/2}$	Revised $K_{I_{min}}$ $MPam^{1/2}$	Comments
1T	529	34	1.242	4.47	3.31	
2T	896	20	1.432	5.04	4.56	
3T	716	20	1.240	4.65	3.42	(a) was not revised because projecting agglomerates were not prominent features
4T	651	30	1.437	4.47	4.07	
5T	708	26	1.211	5.37	3.80	Projecting agglomerates off minor axis
			Average	4.8	3.8	

fracture. Therefore, the cracks are deflected over, under and around the hummocks. The preferred paths are those in which the grains are elongated parallel to the fracture surface. In these paths, those grains oriented perpendicular to the fracture surface pull out or fracture, as suggested by Bowen[5,6], contributing to the fracture resistance.

The ellipticity of the dark regions remains to be explained. The tensile specimens were six inches long and were cut from hot pressed billets, 6 x 6 x 1 in. The fracture surfaces were roughly perpendicular to the long axes of the specimens so that each surface can be considered to contain axes perpendicular and parallel to the hot pressing direction. It is well known that the average strengths of specimens cut with the long axes parallel to the hot pressing direction are lower than those of specimens cut perpendicular to the hot pressing direction[17]. Therefore, one possible explanation is that the ellipticity is caused by differences in the fracture energies for crack propagation in the directions perpendicular and parallel to the hot pressing direction.

An alternative explanation of the ellipticity of the dark areas is that the flaws are elongated and that the cracks tend to propagate in all directions from the flaw preserving this elongation. Examination of the flaws revealed that they were rather irregular in shape and were more or less elongated. In some cases the ellipticity of the dark region seemed to correspond to that of the flaw. However, it should be noted that the flaws may be elongated perpendicular to the hot pressing direction so that the suggested explanations may not be independent of each other.

The large variations in eccentricity (a/c) of the dark region indicate the possibility of rather large variations in the fracture

energy anisotropy and the flaw anisotropy from specimen to specimen. Therefore, the present evidence is most useful for defining the nature of the problem but is not sufficient to permit conclusions to be drawn. In any case, Lange[14] and Miller et al.[3] both observed a 20% reduction in the strengths of specimens fractured in the weak direction compared with the strong direction. The average difference between $K_{I_{max}}$ and $K_{I_{min}}$ is consistent with this difference in the strengths.

It is also interesting to note that the fracture mirror (crack branching) boundaries are circular or almost circular indicating that the ellipticity in the early stages of crack propagation does not extend to the later stages. This observation, together with the variations in the mode of fracture, indicates that the mechanism of fracture at branching is not necessarily the same as that near the fracture origin. This has implications for the relative sizes of critical flaws and fracture mirrors in various ceramics.

Stress intensity factor vs. percent intergranular fracture

The PIF was determined along the major and minor axes of the ellipses formed by the boundaries of the dark areas. The results were somewhat variable, in part because of variations in the quality of the photographs. Emphasis was placed on determinations along the minor axes because the highest K_I values are observed there.

Two of the resulting curves of K_I vs. PIF are given in Figures 6 and 7. At low values of K_I, the PIF is determined mainly by the characteristics of the particular flaw at the fracture origin which may vary widely as

AD-A065 417 CERAMIC FINISHING CO STATE COLLEGE PA F/G 11/1
FRACTOGRAPHIC INVESTIGATION OF SUBCRITICAL CRACK GROWTH AT INHE--ETC(U)
NOV 78 H P KIRCHNER, R M GRUVER, D M RICHARD N00019-77-C-0328

UNCLASSIFIED NL

2 OF 2
AD
A 065417

END
DATE
FILMED
4-79
DDC

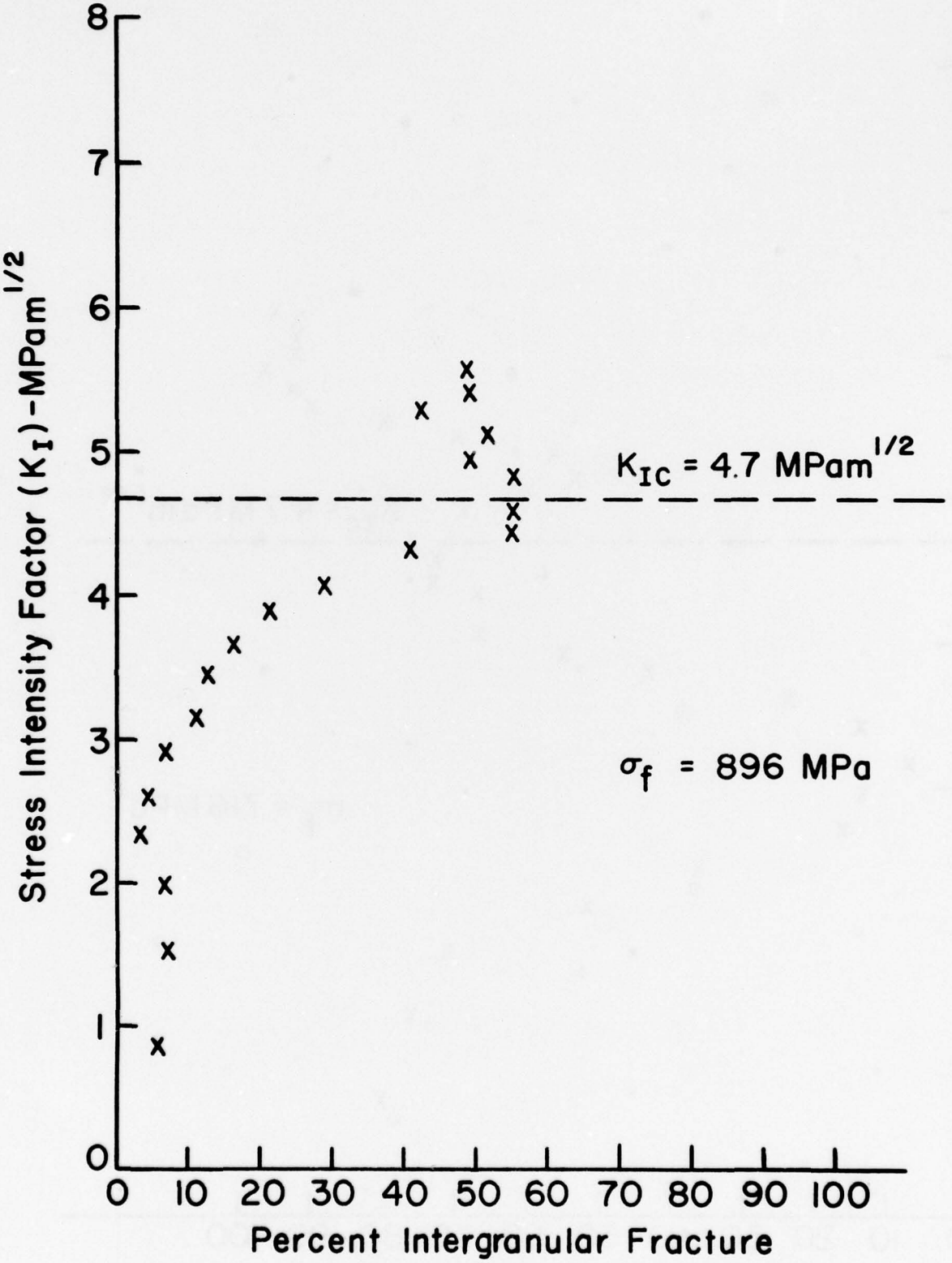

Figure 6 Stress Intensity Factor vs. Percent Intergranular Fracture Specimen 2aT, Minor Axis of Ellipse

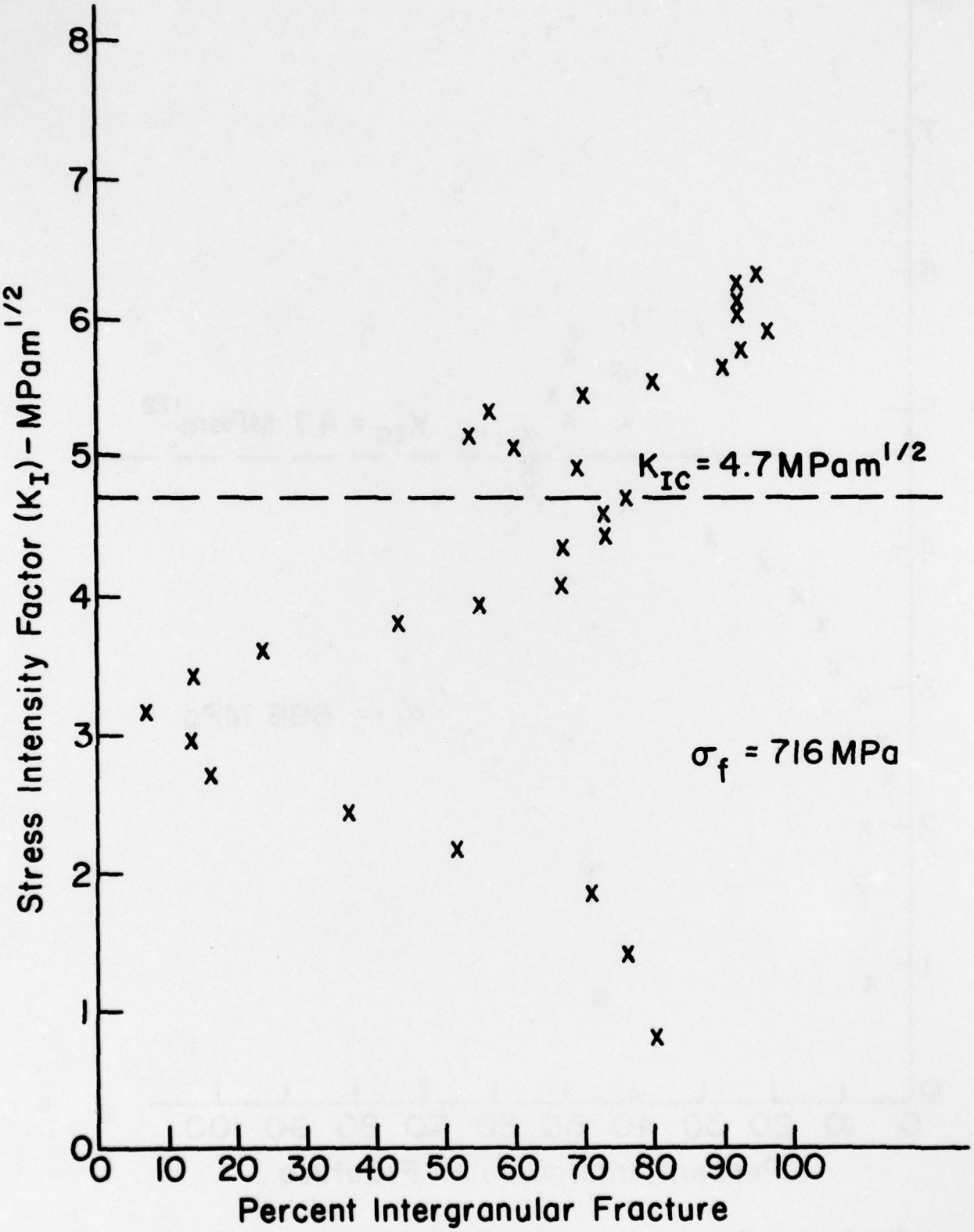

Figure 7 Stress Intensity Factor vs. Percent Intergranular Fracture, Specimen 3T, Minor Axis of Ellipse.

indicated in these figures. However, in both cases the curves pass through low values of PIF (high percentages of transgranular fracture) which are followed by a strong trend toward higher PIF.

These curves confirm that the fracture origins are surrounded by a band of primarily transgranular fracture. In addition, they indicate that $K_I = K_{IC}$ in a region of relatively high PIF. This result is consistent with expectations if crack propagation is inhibited by agglomerates that finally pull out when $K_I = K_{IC}$.

Recent data of Govilla[18] raises some doubt about the correctness of the K_{IC} values chosen for use in analyzing the above data. Govilla tested nominally similar material and observed $K_{IC} = 4.1$ MPam$^{1/2}$ (range 3.9 - 4.4 MPam$^{1/2}$). Analysis on the basis of Govilla's data would lead to some difference in interpretation because the subcritical crack growth boundary would be shifted closer to the outer edge of the dark elliptical region. However, the PIF at 4.1 MPam$^{1/2}$, as indicated in Figures 6 and 7, is well above the value at minimum PIF so that the difference in fracture modes of H.P. silicon nitride and H.P. alumina at criticality is still evident. Despite the availability of the new data it was decided to retain the original interpretation for the following reasons: (1) Govilla stressed that his new data are preliminary, (2) the material used in our investigation was manufactured at a much earlier time (1973) and therefore is more likely to be like the materials used by Petrovic et al[16] and Evans and Wiederhorn than that of Govilla, (3) K_{IC} values of Lange[19] for research specimens having varying percentages of α - Si_3N_4 in the starting powders and, therefore, varying degrees of particle

elongation, ranged from 4.16 to 6.0 $MPam^{1/2}$ so that, considering the fact that NC-132 silicon nitride contains a substantial fraction of elongated grains, it seems unlikely that the NC-132 silicon nitride would have K_{IC} as low as 4.1 $MPam^{1/2}$ and (4) the essential aspects of the interpretation, especially the difference in the fracture mode at the subcritical crack growth boundary compared with that in H.P. alumina, would remain unchanged.

IV. Conclusions

Study of fracture origins, dark ellipses surrounding the fracture origins and the hummocks and depressions has shown that there is an orderly sequence of fracture features observed along radii extending from internal fracture origins in H.P. Si_3N_4. Initially, the cracks grow from the fracture origin by transgranular fracture. Similar results were obtained previously for H.P. alumina and 96% alumina[12,13]. Apparently, as the crack accelerates with increasing K_I, there is insufficient time for transgranular fracture to occur and the crack is forced to find another path. Based on our previous observations in alumina ceramics we would have expected simply increased intergranular fracture. However, this appears to be prevented with the result that the crack diverges from the average fracture plane forming a continuing series of hummocks and depressions. Present evidence indicates that these features are formed because of the presence of fracture resistant agglomerates. This fracture resistance may arise because of the presence of elongated crystals which may tend to bind the agglomerates together. Such an explanation is consistent with the increased strength of H.P. Si_3N_4 bodies derived from high alpha powders which form elongated crystals on conversion to beta silicon nitride[5,6].

Based on these observations a criterion for locating the subcritical crack growth boundary in a particular silicon nitride, can be suggested. First, the dark elliptical region formed by transgranular fracture should be outlined. Then, the hummocks formed along the extensions of the minor

axis of the ellipse should be located. An ellipse of the same eccentricity as the dark region, drawn through the outer edge of the first of these hummocks should coincide approximately with the subcritical crack growth boundary.

Acknowledgements

The writers are pleased to acknowledge helpful discussions with Dr. L. J. Bowen of The Pennsylvania State University and the sponsorship of the Naval Air Systems Command.

References

1. R. M. Gruver, W. A. Sotter and H. P. Kirchner, "Fractography of Ceramics," Ceramic Finishing Company Summary Report, Contract N00019-73-C-0356 (November, 1974).

2. H. P. Kirchner, R. M. Gruver and W. A. Sotter, "Characteristics of Flaws at Fracture Origins and Fracture Stress-Flaw Size Relations in Various Ceramics," Mater. Sci. Eng. 22, 147-156 (1976).

3. F. I. Baratta, G. W. Driscoll and R. N. Katz, "Use of Fracture Mechanics and Fractography to Define Surface Finish Requirements for Si_3N_4," from Ceramics for High Performance Applications, Edited by J. J. Burke, A. E. Gorum and R. N. Katz, Brook Hill Publishing Co., Chestnut Hill, MA (1974), pp. 445-576.

4. D. G. Miller, et al., "Brittle Materials Design, High Temperature Gas Turbine Material Technology," Vol. IV, Westinghouse Electric Corp. Final Report, AMMRC CTR 76-32, Contract DAAG 46-71-C-0162, (December, 1976).

5. L. J. Bowen and T. G. Carruthers, "Development of Mechanical Strength in Silicon Nitride," J. Mater. Sci. 13, 684-687 (1978).

6. L. J. Bowen, Ph.D. Thesis, U. of Leeds, (1977).

7. M. E. Gulden and A. G. Metcalfe, "Stress Corrosion of Silicon Nitride," J. Amer. Ceram. Soc. 59 (9-10), 391-396 (1976).

8. A. G. Evans and G. Tappin, "Effects of Microstructure on the Stress to Propagate Inherent Flaws," Proc. Brit. Ceram. Soc. 20, 275-297, (June, 1972).

9. G. K. Bansal, W. H. Duckworth and D. W. Niesz, "Strength-Size Relations in Ceramic Materials: Investigation of an Alumina Ceramic," J. Amer. Ceram. Soc. 59 (11-12), 472-478 (1976).

10. G. K. Bansal and W. H. Duckworth, "Fracture Stress as Related to Flaw and Fracture Mirror Sizes," J. Amer. Ceram. Soc. 60 (7-8), 304-310 (1977).

11. R. W. Rice, Comment on "Fracture Stress as Related to Flaw and Fracture Mirror Sizes," J. Amer. Ceram. Soc. 61 (9-10), 466-467 (1978).

12. H. P. Kirchner and R. M. Gruver, "A Fractographic Criterion for Subcritical Crack Growth Boundaries in Hot Pressed Alumina," Submitted for publication.

13. H. P. Kirchner and R. M. Gruver, "Fractographic Criteria for Subcritical Crack Growth Boundaries in 96% Alumina," To be submitted for publication.

14. G. K. Bansal, "Effect of Flaw Shape on Strength of Ceramics," J. Amer. Ceram. Soc. 59 (1-2), 87-88 (1976).

15. A. G. Evans and S. M. Wiederhorn, "Crack Propagation and Failure Prediction in Silicon Nitride at Elevated Temperatures," J. Mater. Sci. 9, 270-278 (1974).

16. J. J. Petrovic, L. A. Jacobson, P. K. Talty and A. K. Vasudevan, "Controlled Surface Flaws in Hot-Pressed Si_3N_4," J. Amer. Ceram. Soc., 58 (3-4), 113-116 (1975).

17. F. F. Lange, "Relation Between Strength, Fracture Energy and Microstructure of Hot-Pressed Si_3N_4," J. Amer. Ceram. Soc. 56 (10), 518-522 (1973).

18. R. K. Govilla, "Methodology for Ceramic Life Prediction and Related Proof Testing," Ford Motor Company Interim Report AMMRC TR 78-29, Contract DAAG-46-77-C-0028 (July, 1978).

19. F. F. Lange, "Fracture Toughness of Si_3N_4 as a Function of the Initial α - Phase Content", Rockwell International Science Center Technical Report No. 4 (SC5117.4 TR) Contract N00014-77-C-0441 (July, 1978).

General Conclusions and Recommendations

The suggested fractographic criteria for subcritical crack growth boundaries in H.P. alumina, 96% alumina and H.P. silicon nitride are given in Table I. Comparison of these criteria indicates that in each case the transition from subcritical to critical crack growth occurs as a result of fracture mechanisms that are unique to the particular material. The present results indicate that these differences arise as a result of differences in fracture energy anisotropy, grain size, grain shape and spatial variations in the degree of preferred orientation of the grains.

The present results have implications that range far beyond the solution of the problem of locating subcritical crack growth boundaries in these particular materials. Some of these implications are indicated by the following recommendations for future research in which the techniques developed in this program can be applied:

1. Development of improved methods for evaluating K_{IC} in polycrystalline ceramics that take into consideration the localized variations in material properties on the scale of the critical flaws.

2. Determination of the variations in strength controlling fracture mechanisms in various ceramics with variations in temperature and environmental conditions.

3. Further investigations of the relationships between fracture mechanisms in single crystals and grain boundaries and the variations in fracture mechanisms in polycrystalline ceramics.

Table I. Fractographic Criteria for Subcritical Crack Growth Boundaries in Various Polycrystalline Ceramics.

Material	Criterion
H.P. Alumina	The locus of points characterized by minima in PIF near K_{IC} for fracture on $\overline{1}\overline{1}26$ fracture planes ($K_{IC} \cong 4.3$ MPam$^{1/2}$).
96% Alumina	Type I (Criticality occurs at K_I values near polycrystalline K_{IC}) The locus of points characterized by minima in PIF near K_{IC} for fracture on $\overline{1}\overline{1}26$ fracture planes ($K_{IC} \cong 4.3$ MPam$^{1/2}$).
	Type II (Criticality occurs at K_I values less than polycrystalline K_{IC}) The locus of points at which K_I equals the K_I value at which the strong trend toward high values of PIF begins.
H.P. Silicon Nitride	The locus of points on the curve formed by joining the outer extremes of the first hummocks and depressions observed near the minor axes of dark ellipses formed by transgranular fracture by ellipses of the same eccentricities and orientations as the dark ellipses.

4. Investigation of mechanisms of toughening of ceramics.

5. Development of improved understanding of the relationships between the early stages of crack propagation and the later stages; that is, between subcritical and critical crack propagation.

6. Investigation of the effects of variations in stress state and crack opening mode on fracture mechanisms.

7. Further investigations of the effects of grain size and crack velocity on fracture mechanisms.

DISTRIBUTION LIST

Naval Air Systems Command (9)
AIR-52032
Washington, D. C. 20360

Office of Naval Research
Washington, D. C. 20360
Attn: Code 471

Inorganic Materials Division (2)
Institute for Materials Res.
National Bureau of Standards
Washington, D. C. 20234

Defense Metals & Ceramics
Information Center
Battelle Memorial Institute
505 King Avenue
Columbus, Ohio 43201

Air Force Materials Lab. (7)
Wright-Patterson AFB
Dayton, Ohio 45433
Attn: LMC 1
LMD 1
LMN 1
LAE 1
LAM 1
LAY 1
LAT 1

Atomic Energy Commission
Tech. Information Service
P. O. Box 62
Oak Ridge, Tenn. 37830

Marshall Space Flight Ctr.
Huntsville, Ala. 35812
Attn: D. W. Gates

Goddard Space Flight Ctr.
Greenbelt, Md. 20771
Attn: A. G. Eubanks

Physical Sciences Lab.
Redstone Arsenal
Huntsville, Ala. 35809

Naval Air Systems Command (12)
Washington, D. C. 20360
Attn: NAVAIR-604 (Library
and DDC)

Materials Sciences & Eng.
Laboratory
Stanford Research Institute
Menlo Park, Calif. 94025

Battelle Memorial Institute
505 King Avenue
Columbus, Ohio 43201

IIT Research Institute
10 West 35th Street
Chicago, Illinois 60616
Attn: Ceramics Division

Materials Research Corp.
Orangeburg, New York
10962

Naval Research Laboratory (3)
Washington, D. C. 20390
Attn: Code 6000 1
6136 1
8430 1

NASA Headquarters
Washington, D. C. 20546
Attn: J. J. Gangler, RRM

Lewis Research Center
21000 Brookpark Road
Cleveland, Ohio 44135
Attn: Dr. Hubert Probst

Materials Sciences Lab.
Army Matls. & Mech. Res. Ctr.
Watertown, Mass. 02172

Electronic Parts & Matls. Div.
U.S. Army Electronics,
R & D Laboratory
Fort Monmouth, N.J. 07703
Attn: S. DiVita

Structure & Mechanics Lab.
Redstone Arsenal
Huntsville, Ala. 35809

The Boeing Company
Materials Department
P. O. Box 3868
Seattle, Wash. 98124

Dept. of Materials Science and
Mineral Engineering
University of California
Berkeley, Calif. 94720

Coors Porcelain Company
600 Ninth Street
Golden, Col. 80401
Attn: Research Dept.

Materials Research Ctr.
Lehigh University
Bethlehem, Pa. 18015

Electronics Division
Union Carbide Corp.
P. O. Box 23017
San Diego, Calif. 92100

Midwest Research Institute
425 Volker Boulevard
Kansas City, Mo. 64110
Attn: G. Gross

Dept. of Ceramic Eng.
University of Utah
Salt Lake City, Utah 84412

School of Ceramics
Rutgers, The State Univ.
New Brunswick, N.J. 08903

Southern Research Institute
2000 Ninth Avenue South
Birmingham, Ala. 35205

Materials Research Lab.
Penn. State University
University Park, Pa. 16802
Attn: Prof. R. Roy

Honeywell Research Ctr.
500 Washington Ave., South
Hopkins, Minn. 55343
Attn: Dr. R. J. Stokes

Research Department
Corning Glass Works
Corning, N.Y. 14832

A. C. Spark Plug Div.
General Motors Corp.
Flint, Michigan 48556

Dept. of Metallurgy
Massachusetts Inst. of Tech.
Cambridge, Mass. 02139

Dept. of Metallurgy
Case-Western Reserve Univ.
Cleveland, Ohio 44106
Attn: Dr. A. H. Heuer

Research and Dev. Division
Carborundum *Company*
Niagara Falls, N.Y. 14302

Bell Aerosystems Company
Buffalo, N.Y. 14240
Attn: Materials Res. &
Structural Sys. Dept.

Materials Sciences Lab.
United Aircraft Corp.
East Hartford, Conn. 06101

Metal. & Ceramics Res. Dept.
General Electric R&D Lab.
P. O. Box 8
Schenectady, N.Y. 12301
Attn: Dr. J. Burke

Engineering Experiment St.
Georgia Inst. of Technology
Atlanta, Ga. 30332
Attn: J. D. Walton

Eastman Kodak Company
A&O Division Research Dept.
400 Plymouth Avenue North
Rochester, N.Y. 14650
Attn: Mr. S. E. Hatch

Glass-Ceramics Research Dept.
Corning Glass Works
Corning, N.Y. 14832
Attn: J. F. MacDowell

State University of N. Y.
College of Cer. at Alfred Univ.
Alfred, N.Y. 14802

American Lava Corp.
Chattanooga, Tenn. 37405
Attn: R. D. Dillender

Hughes Aircraft Company
Aerospace Group
R&D Division
Culver City, Calif. 90130

Space Sciences Laboratory
General Electric Company
P. O. Box 8555
Philadelphia, Pa. 19101

Honeywell, Inc.
Ceramics Department
1685 Douglas Drive
Minneapolis, Minn. 55422
Attn: Dr. W. B. Harrison

Westinghouse Research Labs
Beulah Road
Churchill Borough
Pittsburgh, Pa. 15235

Union Carbide Corp.
Parma Technical Center
P. O. Box 6116
Cleveland, Ohio 44101

Battelle Memorial Institute
Pacific Northwest Laboratory
Richland, Wash. 99352
Attn: Dr. T. Chikalla

Dr. Peter Gielisse
Materials Engineering
University of Rhode Island
Kingston, R. I. 02881

University of Kentucky
Dept. of Metallurgical Eng.
Lexington, Kentucky 40506

National Beryllia Corp.
Greenwood Avenue
Haskell, N.J. 07420

College of Earth & Min. Sci.
Penn State University
University Park, Pa. 16802
Attn: Prof. R. C. Bradt

Raytheon Company
Research Division
28 Seyon Street
Waltham, Mass. 02154
Attn: Dr. J. Pappis

McDonnell-Douglas Company
Missile & Space Sys. Div.
3000 Ocean Park Boulevard
Santa Monica, Calif. 90405

Dept. of Engineering
University of California
Los Angeles, Calif. 90024
Attn: Prof. W. J. Knapp

Research Library
Owens-Illinois Tech. Center
1700 N. Westwood Avenue
Toledo, Ohio 43607

Dept. of Engineering Res.
North Carolina State Univ.
Raleigh, N.C. 22055
Attn: Dr. H. Palmour

Tyco Laboratories
Special Products Division
Bear Hill
Waltham, Mass. 02154

Prof. W. A. Tiller
Dept. of Materials Science
Sanford University
Palo Alto, Calif. 94305

Aerospace Corporation
Materials Laboratory
P. O. Box 95085
Los Angeles, Calif. 90045

Norton Company
1 New Bond Street
Worcester, Mass. 01606

ARO Durham
Box CM, Duke Station
Durham, N. C. 27706
Attn: CRDARD-MC

Turbine Research Dept.
Car Research
Product Development Group
Ford Motor Company
20000 Rotunda Drive
Dearborn, Mi. 48121
Attn: E. A. Fisher

Aluminum Company of America
1200 Ring Building
Washington, D. C. 20036
Attn: G. B. Barthold

Dept. of Matls. Sci. & Eng.
Cornell University
Ithaca, N. Y. 14850

Fiber Materials, Inc.
Broadway and Main Street
Graniteville, Mass. 01829

DCI Deposits & Composites, Inc.
1821 Michael Faraday Drive
Reston, Va. 22090
Attn: Dr. R. E. Engdahl

E. I. DuPont de Nemours & Co.
Experimental Station, Bldg. 302
Wilmington, Del. 19898
Attn: Dr. E. J. Kobetich

Mr. F. G. Stroke
PPG Industries, Inc.
One Gateway Center
Pittsburgh, Pa. 15222